GAIN CHARACTERISTICS OF A Nd^{3+}-GLASS LASER AMPLIFIER

GAIN CHARACTERISTICS OF A Nd^{3+}-GLASS LASER AMPLIFIER

by

H. STANLEY DOUGLASS, B.Sc.

A Thesis

Submitted to the Faculty of Graduate Studies

in Partial Fulfilment of the Requirements

for the Degree

Master of Science

McMaster University

March 1969

MASTER OF SCIENCE (1969)
(Physics)

McMASTER UNIVERSITY
Hamilton, Ontario

TITLE: Gain Characteristics of a Nd^{3+}-Glass Laser Amplifier

AUTHOR: H. Stanley Douglass, B.Sc. (University of New Brunswick)

SUPERVISOR: Professor C. K. Campbell

NUMBER OF PAGES: 75, viii

SCOPE AND CONTENTS:

A rate equation model of the Nd^{3+}-glass laser amplifier is set up, and, with the aid of certain simplifying assumptions, a solution is obtained. From this solution, models relating the power and energy of the laser amplifier to its input pumping energy are constructed. The energy gain model thus obtained is tested by experiment, the procedure of which is described in detail in this thesis. The results of this test indicate excellent agreement, within the limitations of the experiment.

ABSTRACT

A model relating the gain of a Nd^{3+}-glass laser amplifier to its input pumping energy is developed in this thesis. This model, which is based on the Nd^{3+} rate equations, is tested experimentally, using a giant pulse as the input to the amplifier. The results of these experiments conform well to the model.

ACKNOWLEDGEMENTS

The author is indebted to Dr. C. K. Campbell for providing the impetus for this study, and for his encouragement and helpful suggestions during the course of its execution.

Dr. K. O. Hill, during the course of his graduate work at McMaster, was a friend and selfless helper.

To all who were involved in the manufacture of the apparatus, especially in the machine shop, I express my appreciation.

To Mr. Illya Mashalidis, who assisted with the preliminary gain measurements, I extend my thanks.

I am indebted to the National Research Council of Canada for its support during the academic year 1967-68, in the form of a bursary.

I am also indebted to McMaster University, for its support during the remainder of the time required for this project.

TABLE OF CONTENTS

		PAGE
CHAPTER I:	INTRODUCTION ----------	1
1.1	The Laser Amplifier ----------	1
1.2	Scope of This Thesis ----------	2
CHAPTER II:	ANALYTICAL DESCRIPTION OF A LASER AMPLIFIER ----	4
2.1	Introduction: The Nd^{3+}-in-Glass Laser ---------	4
2.2	Formulation of the Rate Equations for the Laser Amplifier ----------	6
2.3	Solution of the Rate Equations ----------	11
2.4	Amplifier Solution for a Lorentzian Input Pulse -	13
2.5	Total Energy Gain at Saturation ----------	16
2.6	Relation of Pump Energy to Population Inversion -	17
2.7	Summary of Assumptions Used in this Chapter ----	18
CHAPTER III:	EXPERIMENTAL APPARATUS AND PROCEDURE ----------	21
3.1	The Optical System ----------	21
3.1.1	The Laser Oscillator ----------	21
3.1.2	Beam Splitters, Laser Amplifier, Detector and Autocollimator ----------	24
3.2	The Electrical System ----------	25
3.2.1	The GNB Laser Energy Sobsystem ----------	28
3.2.2	The Synchronizing Subsystem ----------	29
3.2.3	The Detection Subsystem ----------	32

PAGE

3.3 Procedures ---------- 34

3.3.1 Procedure for Determining Amplifier Pump Energy ---------- 36

3.3.2 Procedure for Measuring Energy Gain --------- 37

3.3.3 Power Gain Measurement Procedure ---------- 40

CHAPTER IV: EXPERIMENTAL RESULTS ---------- 41

4.1 Relation of Amplifier Pump Energy to Electrical Energy Input to Flashlamp ---------- 41

4.2 Energy Gain Results ---------- 41

4.3 Result of the Attempt to Measure Power Gain --- 51

CHAPTER V: CONCLUSIONS ---------- 56

APPENDIX I JUSTIFICATION OF THE STATEMENT, "b << a" ------- 60

APPENDIX II COMPARISON OF $\frac{N_2}{g_2}$ and $\frac{N_4}{g_4}$ ---------- 61

APPENDIX III DATA ---------- 63

APPENDIX IV COMPUTER PROGRAMS ---------- 73

REFERENCES 74

LIST OF ILLUSTRATIONS

FIGURE		PAGE
2-1	Nd^{3+} Energy Level Scheme ----------	5
2-2	Splitting of the $^4F_{3/2}$ and $^4I_{11/2}$ Levels ----------	8
2-3	Comparison of a Lorentzian Pulse Shape with the actual Shape of the Giant Pulse Used ----------	14
3-1	Photograph of the Entire Optical System ----------	22
3-2	Photograph of the GNB Laser Energy Subsystem --------	26
3-3	Photograph of the Sychronizing Unit ----------	27
3-4	Diagram of the GNB Laser Energy Subsystem ----------	30
3-5	Diagram of the Synchronizing Subsystem ----------	31
3-6	Diagram of the Detection Subsystem ----------	35
4-1	Relation of the Amplifier Pump Energy E to the Electrical Energy Input to the Flashlamp ----------	42
4-2	Typical Set of Five Oscillograms, From which Energy Gain Measurements were made ----------	43
4-3	Experimental Relation Between First Pulse Heights and Unamplified Pulse Energies ----------	45
4-4	Energy Gain Results of the Laser Amplifier, with Input Pulse Energies of 20-50 Millijoules ----------	46
4-5	A Second Experimental Relation Between First Pulse Heights and Unamplified Pulse Energies ----------	48
4-6	Experimental Relation Between Second Pulse Areas and Amplified Pulse Energies ----------	50

FIGURE PAGE

4-7 Energy Gain Results of the Laser Amplifier, with Input Pulse Energies of 0.7-1.4 Millijoules ---------- 51

4-8 A Second Experimental Relation Between Second Pulse Areas and Amplified Pulse Energies ---------- 53

4-9 Energy Gain Results of the Laser Amplifier, with Input Pulse Energies of 0.05 - 0.12 Millijoules ------ 54

5-1 Energy Gain Results for the 20 - 50 Millijoule Input Pulse Energy Case, Shown with Fitted Theoretical Curves Corresponding to Various Values of the Stimulated Emission Cross Section σ ---------- 57

CHAPTER I

INTRODUCTION

1.1 The Laser Amplifier:

The name "laser" arises from the principle upon which the device is based, namely, light, amplification by the stimulated emission of radiation. This amplification takes place in a medium in which a sufficient number of a particular ion are in a metastable state above the ground state. A photon beam of the correct frequency, passing through such a medium, stimulates this ion to release its energy to the beam, thus amplifying it.

The ions may be raised to the upper metastable state by either electrical or optical means; in the case of solid state lasers, such as the Nd^{3+}-in-glass laser used in this experiment, optical pumping is used. In the case of optical pumping, the ions are first pumped to the "pumping levels", a number of closely-spaced levels above the upper metastable state, which quickly decay to that state. If the laser action takes place between the upper metastable state and the ground state, we describe the system as a three-level laser. This is the case with the ruby laser, in which Cr^{3+} is the active ion. If, however, the laser action occurs between the upper metastable state and a second, lower state also above the ground state, the system is described as a four-level laser. This is the case with the Nd^{3+}-in-glass laser described in this thesis.

The term "laser" is commonly used to mean the system comprised by an optical cavity containing the optically active medium just described.

If the Q of this cavity is "spoiled" except for a few nanoseconds, a large overpopulation of the upper state results, and the energy is released in a single "giant pulse". This "Q-spoiling" may be accomplished by any one of several techniques, involving electrical, chemical, or mechanical shutters placed within the cavity.

In studying the gain characteristics of the laser amplifier, i.e. the optically active medium by itself, the input beam to the amplifier is usually chosen to be a giant pulse, generated by a Q-switched laser. This choice is made for two reasons: first, because of the higher powers attainable, and second, because of the ease with which the energy in the giant pulse can be controlled, i.e., by controlling the pumping energy.

Studies of the gain characteristics (i.e., variation of gain with pumping energy) of a three-level solid state laser, namely, ruby were made in 1965 by Steele and Davis[14]. Their results indicated essential agreement between experimental power gain, and power gain as calculated from the solution of the rate equations. The subject of the present thesis is the study of the gain characteristics of a four-level solid state laser, namely, an Nd^{3+}-in-glass laser.

1.2 Scope of This Thesis:

The first part of this thesis is chiefly concerned with the construction of an analytical model of the four-level solid state laser amplifier. This construction is based primarily upon two sources. The first of these is the description presented by Hill[6], of the four-level

solid state laser, its rate equations, and their solution as achieved by means of certain simplifying assumptions. The second source is Steele's[13] work relating the solution of the three-level laser rate equations to the amplifier gain.

The next part of this thesis deals with the experimental method used to test this analytical model. The final part, Chapters 4 and 5, illustrate the agreement that is obtained, and outline the consequences that can be inferred from it.

It is hoped that this thesis will prove useful, not only in the development of the theory and its experimental testing, but also (as seen particularly in Chapter 3) in assisting future investigators to circumvent some of the technical difficulties that can arise.

CHAPTER II

ANALYTICAL DESCRIPTION OF A LASER AMPLIFIER

2.1 Introduction: The Nd^{3+}-in-Glass Laser:

The rare earth ion Nd^{3+} is the most popular of the four-level laser ions for several reasons. First, its terminal level is high enough above the ground level, so that is is sparsely populated at room temperature. Thus, pumping to obtain a population inversion is relatively easy. Second, it can be used in a number of different host lattices to obtain laser action. Such crystals as $CaWO_4:Nd^{3+}$, $SrWO_4:Nd^{3+}$, $SrMoO_4:Nd^{3+}$, and $Ca(NbO_3)_2:Nd^{3+}$ have all been used to produce highly monochromatic (spectral width approximately 0.1 Angstrom) laser beams at low power levels[8]. Finally, and most importantly as regards this thesis, the Nd^{3+} ion imbedded in glass can be used to attain laser action at very high power levels. Powers in excess of a gigawatt per square centimeter have been reported[1].

The transition employed in the Nd^{3+}-glass laser is the $^4F_{3/2} \rightarrow {}^4I_{11/2}$ transition (1.06 microns), as indicated in the energy level scheme for Nd^{3+}, Figure (2-1). Since this is a 4f-4f transition, it is strictly parity forbidden in the case of the free Nd^{3+} ion. The fact that it does occur may be explained in terms of a mixing of states of opposite parity, due to the non-centrosymmetric portions of the micro-fields from surrounding ions. If this mixing is small, it may account for the fact that the upper laser level lifetime is hundreds of micro-seconds at room temperature[6].

Figure (2-1)

Nd^{3+} energy level scheme, showing pump levels and laser transition. (After G. H. Diecke: in "Advances in Quantum Electronics", edited by J. R. Singer, Columbia University Press, New York, 1961)

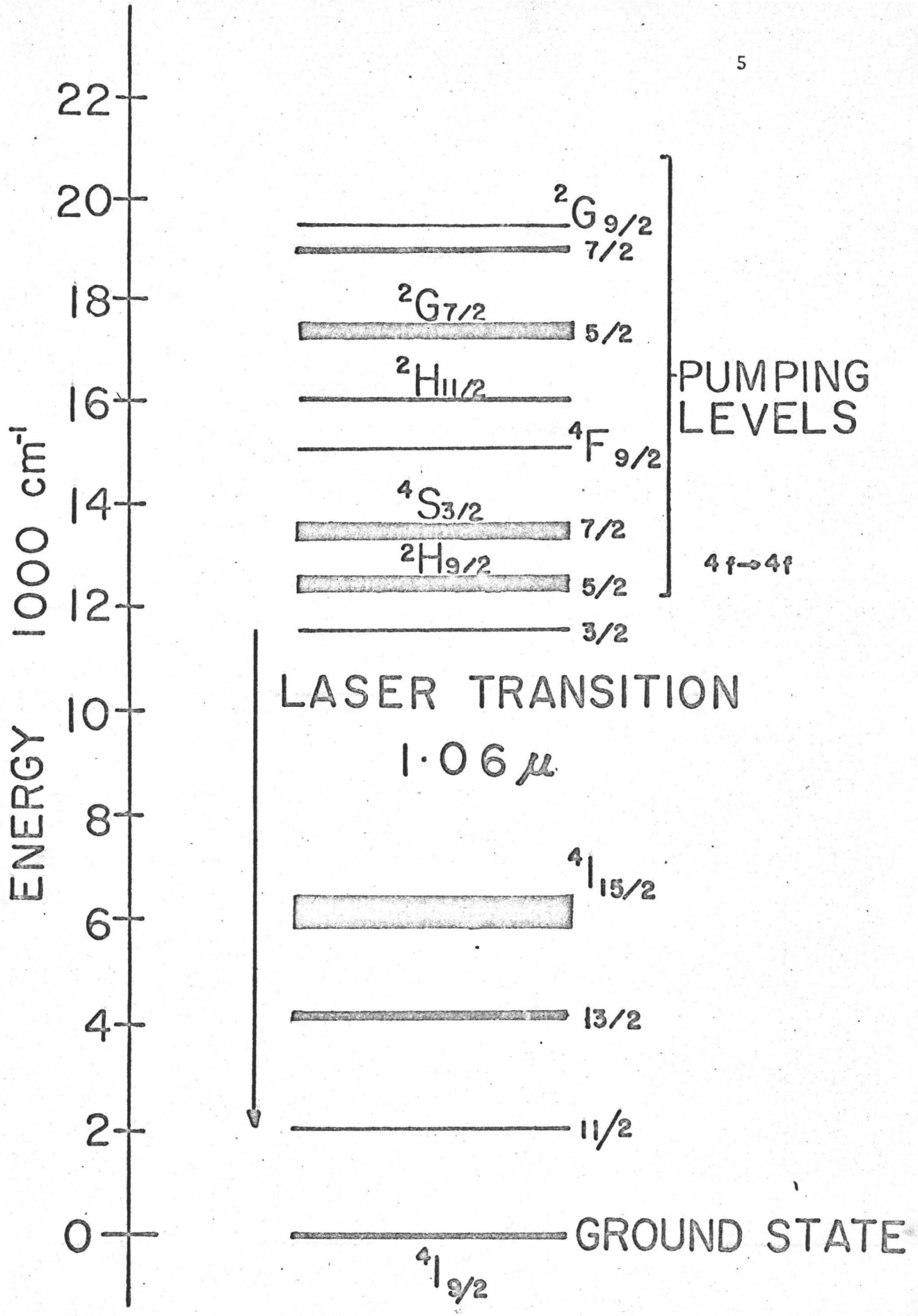
ENERGY 1000 cm⁻¹
22
20
18
16
14
12
10
8
6
4
2
0
$^2G_{9/2}$
7/2
$^2G_{7/2}$
5/2
$^2H_{11/2}$
$^4F_{9/2}$
$^4S_{3/2}$
7/2
$^2H_{9/2}$
5/2
3/2
PUMPING LEVELS
4f→4f
LASER TRANSITION
1·06 μ
$^4I_{15/2}$
13/2
11/2
GROUND STATE
$^4I_{9/2}$

2.2 Formulation of the Rate Equations for the Laser Amplifier:

Consider first the case where the upper and lower laser levels, k and 1, are of equal degeneracy. In this case, the net number of transitions taking place per unit time per unit volume in the laser amplifier medium can be shown to be[6]:

$$\frac{\partial(N_\ell - N_k)}{\partial t} = 2\sigma c\phi(N_k - N_\ell) \qquad (2.2\text{-}1)$$

where N_k = population of level k per unit volume,

N_ℓ = population of level 1 per unit volume,

ϕ = photon density referred to a vacuum,

c = speed of light in a vacuum,

and σ = stimulated emission cross-section of the Nd^{3+} ion.

This expression includes two assumptions. First, the stimulated emission is assumed to monochromatic, which is equivalent to saying that its spectral shape is rectangular and of unit width. Second, it is assumed that the number of spontaneous transitions minus the number of transitions due to continued pumping is negligible, compared to the number of stimulated transitions.

Next, consider the effect of the introduction of a finite lifetime τ for the terminal level ℓ, as is the case with a four-level laser. Then (2.2-1) becomes:

$$\frac{\partial(N_\ell - N_k)}{\partial t} = 2\sigma c\phi(N_k - N_\ell) - \frac{N_\ell}{\tau} \qquad (2.2\text{-}2)$$

We can now see that the number of photons per fixed unit volume -- say, a circular platelet section of the amplifier rod, of area

A and thickness x -- changes at a rate given by:

$$\frac{\partial \phi}{\partial t} = -c \frac{\partial \phi}{\partial x} + \sigma c \phi (N_k - N_\ell) \qquad (2.2\text{-}3)$$

where the term $-c \frac{\partial \phi}{\partial x}$ represents the net rate at which photons flow out of the fixed unit volume.

Finally, we can also see that the rate of change of population of the lower level ℓ is:

$$\frac{\partial N_\ell}{\partial t} = \sigma c \phi (N_k - N_\ell) - \frac{N_\ell}{\tau} \qquad (2.2\text{-}4)$$

Next, we wish to take into consideration the splitting of the upper and lower laser levels, and their degeneracies. The splitting is shown in Figure (2-2). The laser transition is between levels 2 and 4, with populations N_2 and N_4 respectively, and with degeneracies g_2 and g_4 respectively. With these values, (2.2-2), (2.2-3), and (2.2-4) become:

$$\frac{\partial (N_3 + N_4 - N_1 - N_2)}{\partial t} = 2\sigma c \phi \left(\frac{N_2}{g_2} - \frac{N_4}{g_4}\right) - \frac{N_4 + N_3}{\tau}, \qquad (2.2\text{-}5)$$

$$\frac{\partial \phi}{\partial t} = -c \frac{\partial \phi}{\partial x} + \sigma c \phi \left(\frac{N_2}{g_2} - \frac{N_4}{g_4}\right), \qquad (2.2\text{-}6)$$

and

$$\frac{\partial (N_3 + N_4)}{\partial t} = \sigma c \phi \left(\frac{N_2}{g_2} - \frac{N_4}{g_4}\right) - \frac{N_4 + N_3}{\tau}. \qquad (2.2\text{-}7)$$

Our next step is to make use of the thermal equilibrium relating each pair of levels. The Boltzmann equations are:

$$\frac{N_1}{g_1} = \frac{N_2}{g_2} e^{-\frac{\Delta E_1}{KT}}, \text{ and}$$

Figure (2-2)

The splitting of the $^4F_{3/2}$ and $^4I_{11/2}$ energy levels in glass. (After K. O. Hill, "Giant Pulse Evolution in a Nd^{3+}-Glass Q-Switched Laser", McMaster University, 1968)

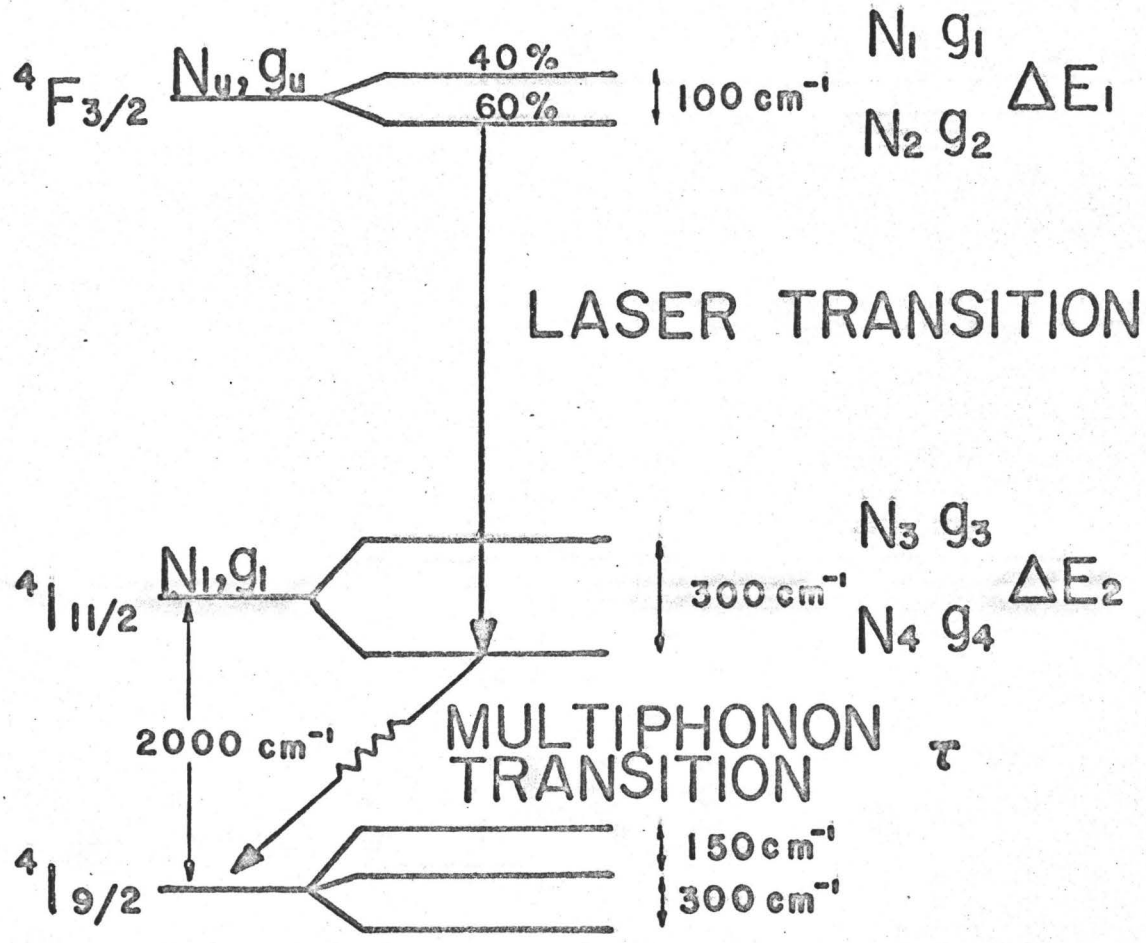
$^4F_{3/2}$
N_u, g_u
40%
60%
100 cm^{-1}
N_1 g_1
N_2 g_2
ΔE_1
LASER TRANSITION
$^4I_{11/2}$
N_l, g_l
300 cm^{-1}
N_3 g_3
N_4 g_4
ΔE_2
2000 cm^{-1}
MULTIPHONON TRANSITION
τ
$^4I_{9/2}$
150 cm^{-1}
300 cm^{-1}

$$\frac{N_3}{g_3} = \frac{N_4}{g_4} e^{-\frac{\Delta E_2}{KT}},$$

where g_1 and g_3 are the degeneracies of levels 1 and 3 respectively. We now define:

$$N = \frac{N_2}{g_2} - \frac{N_4}{g_4}, \quad N_1 = \frac{N_4}{g_4},$$

$$K_1 = \frac{1}{g_4 + g_3 \exp(-\frac{\Delta E_2}{KT})},$$

$$K_2 = \frac{1}{g_2 + g_1 \exp(-\frac{\Delta E_1}{KT})}.$$

The introduction of the parameters K_1 and K_2 is most useful for its minimization of the uncertainty due to our present ignorance of lower level splitting[6]. The manner in which the degeneracies are split between levels 3 and 4 is as yet incompletely known.

Expressing N_1 and N_3 in terms of N_2 and N_4 by means of the Boltzmann equations, and using the definitions just given, we simplify equations (2.2-5), (2.2-6), and (2.2-7) to the following form:

$$\frac{\partial N}{\partial t} = -(K_1 + K_2)\sigma c\phi N + \frac{N_1}{\tau} \qquad (2.2\text{-}8)$$

$$\frac{\partial N_1}{\partial t} = K_1 \sigma c\phi N - \frac{N_1}{\tau} \qquad (2.2\text{-}9)$$

$$\frac{\partial \phi}{\partial t} = -c \frac{\partial \phi}{\partial x} + \sigma c\phi N \qquad (2.2\text{-}10)$$

In order to render these rate equations soluble by analytical means, it is necessary to make a further simplification. If τ is assumed to approach either zero or infinity, the number of equations immediately reduces to two, with a difference of only a factor of two between the two extreme cases. As will be seen in Chapter 4, the half-power width of the giant pulse is roughly 20 nanoseconds. Estimates of τ, on the other hand vary from 60 nanoseconds[10], to 400 nanoseconds[6]. We therefore set τ equal to infinity in the rate equations, which then reduce to the following:

$$\frac{\partial N}{\partial t} = -(K_1 + K_2)\sigma c \phi N \qquad (2.2\text{-}11)$$

$$\frac{\partial \phi}{\partial t} = -c \frac{\partial \phi}{\partial x} + \sigma c \phi N \qquad (2.2\text{-}12)$$

It now remains only to set up the boundary conditions to which these rate equations are subject. We define $x = 0$ as the end of the laser amplifier rod through which the giant pulse enters, and $x = L$ as the end through which it leaves. We further define $t = 0$ to be the time at which the beginning of the giant pulse reaches the position $x = 0$. The photon density before amplification can then be written as:

$$\phi(0, t > 0) = \phi_o(t) \qquad (2.2\text{-}13)$$

The initial population inversion in the amplifier rod can be similarly expressed:

$$N(x, t < 0) = N_o(x) \qquad (2.2\text{-}14)$$

In order to simplify subsequent calculations, we assume uniformity of the amplifier rod, so that $N_o(x)$ becomes simply N_o = constant.

2.3 Solution of the Rate Equations:

Equation (2.2-12) can be immediately solved for N:

$$N = \frac{1}{\sigma c}\left(\frac{1}{\phi}\frac{\partial \phi}{\partial t} + \frac{c}{\phi}\frac{\partial \phi}{\partial x}\right). \qquad (2.3\text{-}1)$$

Substituting this expression into equation (2.2-11), we obtain:

$$\frac{\partial}{\partial t}\left(\frac{1}{\phi}\frac{\partial \phi}{\partial t} + \frac{c}{\phi}\frac{\partial \phi}{\partial x}\right) = -(K_1 + K_2)\sigma c \phi\left(\frac{1}{\phi}\frac{\partial \phi}{\partial t} + \frac{c}{\phi}\frac{\partial \phi}{\partial x}\right)$$

which can be integrated[13] to yield:

$$\phi(x, t) = \frac{\frac{\partial}{\partial t}\left(b(t - x/c)\right)}{(K_1 + K_2)\sigma c[b(t - x/c) + d(x/c)]} \qquad (2.3\text{-}2)$$

where $b(t - x/c)$ and $d(x/c)$ have arisen as constants of integration. An expression for $b(t)$ is now obtained by imposing the boundary condition (2.2-13). This gives:

$$\phi_o(t) = \frac{\frac{\partial}{\partial t} b(t)}{(K_1 + K_2)\sigma c[b(t) + d_o]}$$

where $d_o = d(0/c)$,

which, when integrated, yields:

$$b(t) = d_1 \exp[(K_1 + K_2)\sigma c \int_{-\infty}^{t} \phi_o(t')dt'] - d_o$$

where d_1 is a constant of integration,

t' is a dummy variable of integration.

Substituting this result for b(t) back into equation (2.3-2), we find that:

$$\phi(x, t) = \frac{\phi_o(t - x/c)}{1 + K(x)\ \exp[-(K_1 + K_2)\sigma c \int_{-\infty}^{t-x/c} \phi_o(t')dt']} \qquad \text{---- (2.3-4)}$$

This solution in turn is substituted into equation (2.3-1), which gives:

$$N(x, t) = \frac{-\frac{c}{\sigma c}\left(\frac{\partial K(x)}{\partial x}\right)}{K(x) + \exp[(K_1 + K_2)\sigma c \int_{-\infty}^{t-x/c} \phi_o(t')dt']} \qquad (2.3\text{-}5)$$

Under the second boundary condition (2.2-14), this becomes:

$$N_o = -\frac{1}{\sigma}\left(\frac{1}{1 + K(x)}\right)\frac{\partial K(x)}{\partial x} \ ,$$

and we see, by integrating, that

$$K(x) = d_2 e^{-\sigma N_o x} - 1 \ .$$

And since K(0) = 0, from equation (2.3-4), we see that the constant of integration, d_2, must equal unity.

We now need only substitute K(x) into equations (2.3-4) and (2.3-5) to obtain the complete solutions:

$$\phi(x, t) = \frac{\phi_o(t - x/c)}{1 - [1 - \exp(-\sigma N_o x)]\ \exp[-(K_1+K_2)\sigma c \int_{-\infty}^{t-x/c} \phi_o(t')dt']} \qquad \text{---- (2.3-6)}$$

$$N(x, t) = \frac{N_o \exp(-\sigma N_o x)}{\exp(-\sigma N_o x) + \exp[K_1 + K_2)\sigma c \int_{-\infty}^{t-x/c} \phi_o(t')dt']} \qquad (2.3\text{-}7)$$

2.4 Amplifier Solution for a Lorentzian Input Pulse:

Our next step is to apply these solutions to a particular input pulse shape. From Figure (2-3), we see that it is reasonable to approximate the actual giant pulse shape by one which is Lorentzian in its time development, described by:

$$\phi_o(t) = \frac{DT}{\pi c}\left(\frac{1}{t^2 + T^2}\right) \quad , \tag{2.4-1}$$

where D is the total number of photons per unit area in the beam,

T is the half-width of the pulse.

We can use this approximation to evaluate the integral in (2.3-6) and (2.3-7):

$$\int_{-\infty}^{t-x/c} \phi_o(t')dt' = \frac{DT}{\pi c}\int_{-\infty}^{t-x/c} \frac{dt'}{t'^2 + T^2}$$

$$= \frac{D}{2c}\left[\frac{2}{\pi}\tan^{-1}\left(\frac{t-x/c}{T}\right) + 1\right]$$

$$\simeq \frac{D}{2c}\left[\frac{2}{\pi}\tan^{-1}\frac{t}{T} + 1\right] \tag{2.4-2}$$

And the output photon density obtains explicitly from (2.3-6):

$$\phi_{out}(t) = \frac{\frac{DT}{\pi c}\left(\frac{1}{t^2 + T^2}\right)}{1 - [1 - \exp(-\sigma N_o L)]\exp\left[-(K_1+K_2)\frac{\sigma D}{2}\left(1 + \frac{2}{\pi}\tan^{-1}\frac{t}{T}\right)\right]} \tag{2.4-3}$$

The ratio of the output photon density to the input photon density now gives us the power gain G_p, namely,

Figure (2-3)

(a) Oscillogram showing the variation with time of the amplitude of a typical giant pulse.

(b) Graphical comparison of the intensity measured from this oscillogram with the corresponding intensity of a Lorentzian pulse shape.

(a)

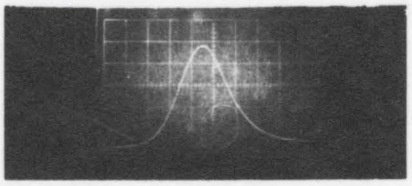

TIME SCALE : 10.0 NANOSECONDS / DIVISION.

(b) GRAPH: COMPARISON WITH LORENTZIAN PULSE SHAPE.

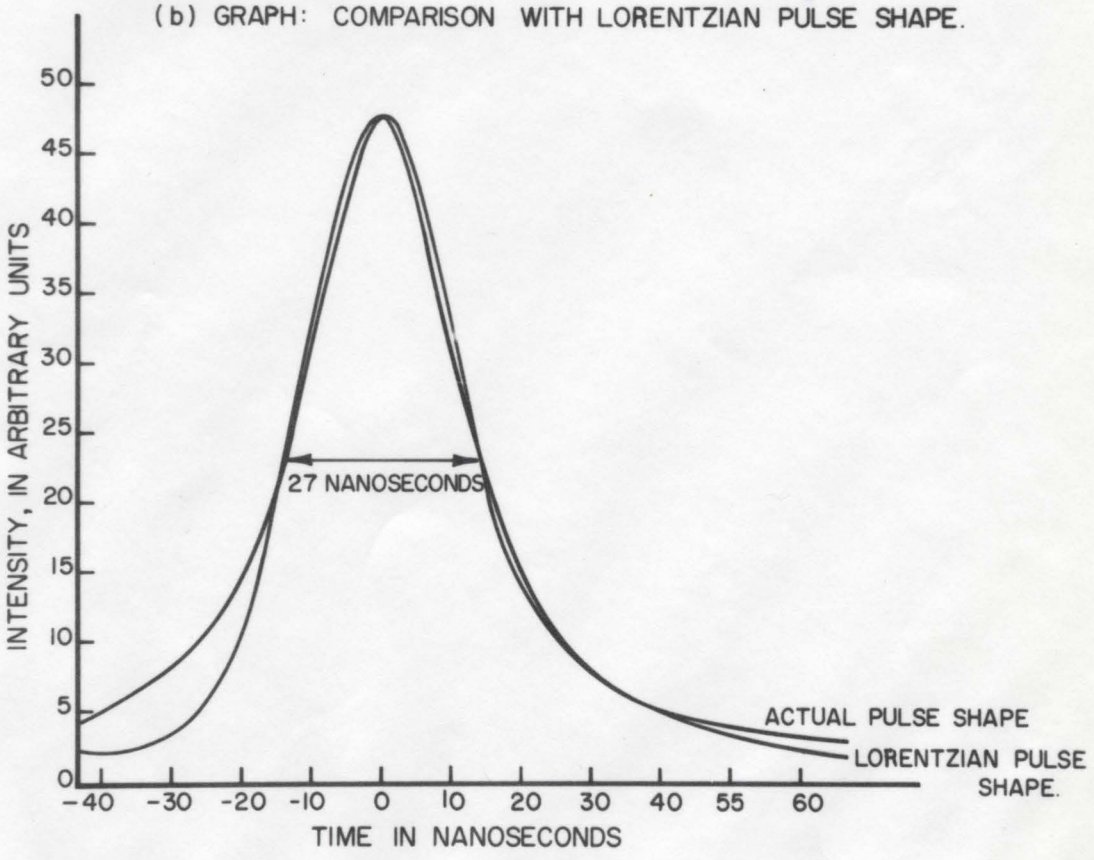

$$G_p = \frac{\phi_{out}}{\phi_o} = \{1 - \exp(-\sigma N_o L)]\ \exp[-(K_1+K_2)\frac{\sigma D}{2}\ (1 + \frac{2}{\pi}\tan^{-1}\frac{t}{T})\ ]\}^{-1}$$

----- (2.4-4)

We can also calculate the total energy gain for the pulse with acceptable accuracy. Since $(K_1+K_2)\frac{\sigma D}{2} << 1$ for the results in this thesis, we begin by making the approximation,

$$\exp[-(K_1+K_2)\frac{\sigma D}{2}\ (1 + \frac{2}{\pi}\tan^{-1}\frac{t}{T})\ ] \approx 1 - (K_1+K_2)\frac{\sigma D}{2}\ (1 + \frac{2}{\pi}\tan^{-1}\frac{t}{T})$$

It is necessary to note at this point that our assumption of a Lorentzian pulse shape has changed our time scale, in that t = 0 now is the time at which the middle, rather than the beginning, of the giant pulse reaches the position x = 0.

We now observe from Figure (2-3) that almost all of the energy of the giant pulse is concentrated between t = -2T and t = 2T. In this region we have, roughly,

$$\tan^{-1}\frac{t}{T} \approx \frac{\pi}{4}\ \frac{t}{T}$$

so that ϕ_{out}, from (2.4-3), simplifies to:

$$\phi_{out} = \frac{\frac{DT}{\pi c}\ (\frac{1}{t^2 + T^2})}{1 - [1 - \exp(-\sigma N_o L)][1 - (K_1+K_2)\frac{\sigma D}{2}\ (1 + \frac{1}{2}\frac{t}{T})\ ]}$$

With these approximations, we can now calculate the total energy gain G_E, namely,

$$G_E \equiv \frac{\int_{-2T}^{2T} \phi_{out}(t)\,dt}{\int_{-2T}^{2T} \phi_o(t)\,dt}$$

$$\equiv \frac{\int_{-2T}^{2T} \frac{dt}{(t^2 + T^2)(a + bt/T)}}{\int_{-2T}^{2T} \frac{dt}{t^2 + T^2}}$$

where $a \equiv 1 - [1 - \exp(-\sigma N_o L)][1 - (K_1 + K_2)\frac{\sigma D}{2}]$

and $b \equiv [1 - \exp(-\sigma N_o L)](K_1 + K_2)(\frac{\sigma D}{4})$.

Then;

$$G_E \equiv \frac{b(\log|a + 2b| - \log|a - 2b|) + a(\tan^{-1}2 - \tan^{-1}-2)}{(a^2 + b^2)(\tan^{-1}2 - \tan^{-1}-2)}$$

----- (2:4-5)

However, in most cases we will find (See Appendix I) that $b << a$, so that we have, finally:

$$G_E \cong \frac{1}{a} \equiv \{1 - [1 - \exp(-\sigma N_o L)][1 - (K_1 + K_2)\frac{\sigma D}{2}]\}^{-1} \qquad (2:4-6)$$

2:5 Total Energy Gain at Saturation:

The term "saturation" is applied to the condition in which all the $^4F_{3/2}$ ions are stimulated to release their energy to the giant pulse as it passes through the amplifier. It will be observed that this condition is not included in the preceding treatment.

The calculation of the total energy gain is extremely simple under saturation conditions:

$$G_E = \frac{\text{number of photons out}}{\text{number of photons in}}$$

$$= \frac{\text{number of photons in} + \text{number of } {}^4F_{3/2} \text{ ions}}{\text{number of photons in}}$$

which is simply

$$G_E = \frac{D + N_o L}{D} \quad . \tag{2.5-1}$$

2.6 Relation of Pump Energy to Population Inversion:

The population inversion in the amplifier rod, before the arrival of the giant pulse, has been written as $N_o = \frac{N_2}{g_2} - \frac{N_4}{g_4}$ in the preciding section. Since $\frac{N_2}{g_2}$ will be of the order of a hundred times $\frac{N_4}{g_4}$ (See Appendix II), we ignore $\frac{N_4}{g_4}$ and write $N_o = \frac{N_2}{g_2}$.

We begin our calculation by assuming that the increment ΔE of the amplifier pump energy is linearly related to the fractional number of ions pumped from the ground state to the pumping levels, and hence to the ${}^4F_{3/2}$ levels. Equivalently,

$$\Delta E = -\gamma \frac{\Delta N_g}{N_g} \quad ,$$

where γ is a constant,

which gives, on integration,

$$N_g = N_{go} \exp(-\gamma E)$$

where N_{go} is the total number of Nd^{3+} ions.

Since the transitions from the pumping levels to the ${}^4F_{3/2}$ levels are fast, we may approximate the number N_k of ions in the ${}^4F_{3/2}$ levels by

$$N_k = N_{go}(1 - e^{-\gamma E}) \quad .$$

We now recall, from Figure (2-2), that only the ions in the lower of the two $^4F_{3/2}$ levels are available for lasing. Since this lower level contains only about 60% of the $^4F_{3/2}$ ions, one would first be led to consider that only this 60% would be available for lasing. However, due to the short relaxation time between these two levels (less than one nanosecond[6]), nearly 100% of the $^4F_{3/2}$ ions are available over the 30 nanosecond duration of the pulse, in the saturation case. Thus:

$$N_o = \frac{N_2}{g_2} = \frac{.60\ N_k}{2} = .30\ N_{go}(1 - e^{-\gamma E})] \qquad (2.6\text{-}1)$$

for the non-saturation calculations,

and

$$N_o = \frac{N_2}{g_2} = \frac{1.00\ N_k}{2} = .50\ N_{go}(1 - e^{-\gamma E}) \qquad (2.6\text{-}2)$$

for the saturation calculation.

2.7 Summary of Assumptions Used in this Chapter:

Several of these assumptions were made in the process of setting up the rate equations. First, we assumed that both the number of spontaneous transitions, and the number of transitions due to continued pumping during the time of passage of the pulse, were negligible compared to the number of stimulated transitions. We further assumed that the transitions involved are predominantly electric dipole transitions. The effect of any cross-relaxation processes that may be operative[10,11] was neglected. Also, we assumed that the photon beam is uniform over its cross-sectional area, i.e., that such non-uniformity as has been shown to exist[7,4] does not significantly alter the results. Further, the spectral shapes of both the spontaneous and the stimulated emission lines were

approximated by rectangular distributions. We note here that this approximation also gives us a first order account of the mode structure. If there are M modes within the spectral width $\Delta\omega$ of the fluorescent line, then on the average, each mode contains $\frac{\phi\Delta\omega}{M}$ photons.

The assumption was made that losses to the photon beam in the amplifier rod, other than losses due to reflectances at the ends of the rod, were negligible. A spectrophotometer run was made to check this assumption; total losses were found to be less than 10% for the whole length of the rod. Furthermore, in measurements of gain, such as comprise this experiment, we are concerned with ratios, so that even this factor nearly disappears, making our assumption very good.

In taking into account the laser level degeneracies and split levels, it was assumed that thermal equilibrium is maintained between these sublevels of the $^4F_{3/2}$ and $^4I_{11/2}$ levels. In reducing the number of rate equations from three to two, it was necessary to replace τ, the lifetime of the $^4I_{11/2}$ state, by infinity. We noted at this stage that this procedure would not alter our results unduly.

In setting up the boundary conditions for these two rate equations, it was assumed that the pumping of the amplifier rod was uniform. This assumption was necessary in order to make calculations manageable, but probably introduced slight inaccuracy for two reasons. First, the end 1/4 inch of the three-inch rod, held in the opaque teflon holder, was not pumped as much as the remaining 2 3/4 inches. Second, the pumping was not uniform radially, but decreased toward the centre of the rod[2].

The solution of the rate equations from this point was exact, but in applying this solution to find power gain, it was necessary to assume an input pulse shape. We assumed a Lorentzian pulse shape; as we saw from Figure (2-3), this was a very reasonable approximation. In the next step, the integration of the input photon density, we neglected the term L/c. The reason for this approximation consists in the fact that $L/c \tilde{-} 1/5$ nanosecond, whereas $T \tilde{-} 10\text{-}20$ nanoseconds.

In relating the pump energy to the population inversion, we neglected the number of ions in the final state, $^4I_{11/2}$, due to thermal equilibrium with the ground state, since this is very small at room temperature. We also neglected the number of ions in the $^4I_{11/2}$ level due to all the spontaneous transitions from the $^4F_{3/2}$ level before Q-switching. This is reasonable (Appendix II), and so long as γE is small, the final comparision between theory and experiment will not be significantly affected.

Next, we assumed that the fraction of ions pumped was linearly related to the increment of pump energy. We then assumed that transitions between the pumping levels and the $^4F_{3/2}$ levels were fast enough to allow us to ignore the proportion of ions left in the pumping levels.

Finally, we assumed that the relaxation time between the two $^4F_{3/2}$ levels was sufficiently short so that all of the ions in the upper level could be made available for lasing, if the input pulse were large enough, i.e., if the saturation condition held.

CHAPTER III

EXPERIMENTAL APPARATUS AND PROCEDURE

3.1 The Optical System:

In our description of the experimental set-up, we first consider the system comprised by those pieces of apparatus directly involved in the creation, amplification, and detection of the giant pulse. Since these operations are all primarily optical processes, we designate this system as the optical system.

The optical system is most easily subdivided for further discussion, according to the particular optical processes involved. Thus, the laser oscillator is responsible for the creation of the giant pulse; the beam splitter's function is to divert part of this pulse for measurement before amplification; the laser amplifier head amplifies the giant pulse; and a TRG detection unit converts it into an electrical signal for measurement after amplification. The oscillator, beam splitter, amplifier, detector, as well as an autocollimator for lining up the system, can all be seen in the photograph, Figure (3-1). The construction and function of each of these pieces of apparatus is discussed in the following subsections.

3.1.1 The Laser Oscillator -

This oscillator, consisting of the rotating prism Q-spoiler, the laser head, and output reflector, has been described and studied in detail by Hill[6].

The Q-spoiler is a Beckman and Whitley Model 402 rotating Porro

FIGURE (3-1)

Photograph of the entire optical system. From left to right, the pieces of apparatus are:

(a) rotating prism Q-spoiler, (b) laser head, (c) output reflector held in a precision holder. These three pieces comprise the laser oscillator.

(d) beam splitter, held in a second precision holder.

(e) second laser head, which constitutes the amplifier.

(f) TRG detection unit.

(g) part of the autocollimator.

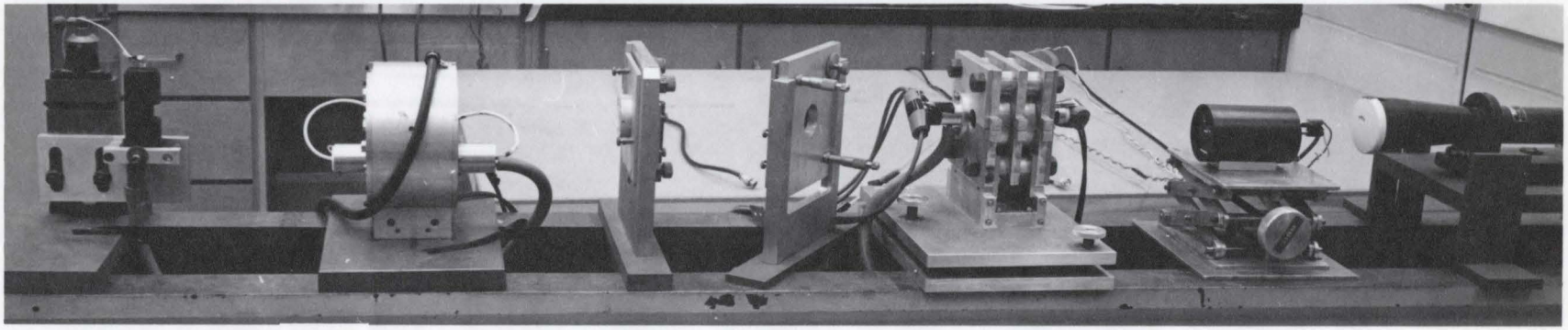

prism, driven by compressed air. Under the maximum 80 psi, it can be driven at speeds up to 1500 rps, although 300 rps was found to be a reasonable value for this experiment. The speed can be monitored by means of a pickup coil built into the rotor housing. This pickup coil, since it can be rotated through 360 degrees with respect to the prism, is also useful for synchronizing the flashlamp pumping pulse with the prism.

The use of a right angle (Porro) prism, rotating about an axis parallel to the prism hypotenuse and perpendicular to the roof edge, serves two purposes. First, any critical alignment problems are automatically eliminated. Second, the cavity length is double the value which obtains if an ordinary rotating mirror is used.

The laser head consists of a highly polished elliptical cylinder with a Kodak Nd^{3+}-doped silicate glass rod at one focus, and an EG&G FX-42C xenon flash-tube at the other. This arrangement results in an energy transfer efficiency, from the flashtube to the laser rod, of up to 50%[(12)]. The flashtube is enclosed in a glass tube to protect the laser rod from possibly damaging ultraviolet radiation. The flashtube and laser rod are both air-cooled from the same compressed air source that drives the rotating prism.

The partially reflecting mirror which serves as the output reflector is a dielectric coated cylindrical glass plate, which is mounted in the precision holder seen in Figure (3-1). This holder has a spring and knurled screw arrangement, which allows manual adjustment of the attitude of the output reflector, to within one second of arc.

3.1.2 Beam Splitters, Laser Amplifier, Detector, and Autocollimator -

A beam splitter is used to divert part of the beam, for measurement before amplification, and for triggering the oscilloscope. This beam splitter consists of a plate of glass held at 45 degrees to the direction of the beam. The holder for this plate is basically the same in design as that used for the output reflector of the laser oscillator.

The second laser head, which constitutes the laser amplifier, is based on the same design as the first laser head, except in two respects. First, the ellipse is horizontal, with the flashtube beside the laser rod, rather than vertical, with the flashtube under the rod. Second, the base consists of two plates rather than one. The upper plate rests on the lower plate, which is fixed firmly to the lathebed, by means of three knurled screws. Two of these screws are pointed, one to fit into a conical indentation, and one to fit into a V-cut groove, in the lower plate; the third screw is rounded. This arrangement allows complete freedom in adjusting the attitude and height of the laser head, by means of the knurled screws, while keeping its lateral position fixed. Thus, alignment of the amplifier rod with the beam from the oscillator is rendered relatively simple. This is especially important in the case of a Brewster angle amplifier rod.

The detector, a TRG Model 101, is the horizontal black cylinder seen in Figure (3-1). It consists of an input cone, into which the laser is fired, and a reference cone connected to it by means of a thermopile. Since the beam is almost entirely absorbed in the input cone due to the Mendenhall Wedge Effect, the potential difference across the thermopile

is a measure of the total energy in the beam. A beam splitter located just in front of the input cone, however, diverts 20% of the beam energy to a fast response photodiode circuit. This circuit converts the intensity variation of the pulse into a measureable electrical signal.

The autocollimator is an optical telescope, with a cross hair and light source arrangement that makes it possible to line up the normal to any optical surface, with the optic axis of the telescope, to within one second of arc. We see, from Figure (3-1), that the use of this autocollimator necessitates that we assemble the optical system from left to right, aligning each piece of apparatus as it is put in place.

3.2 The Electrical System:

This section deals with those parts of the apparatus which are not included in the optical system. Since the functions of these pieces of apparatus are entirely electrical, we designate them collectively as the electrical system. For convenience, we divide this electrical system into several subsystems.

First, there is the GNB laser energy subsystem (Model 20-002), shown in Figure (3-2), which provides the electrical energy for the xenon flashtubes in the laser heads. This subsystem also includes the circuit for triggering the flashtubes.

Second, there is the synchronizing unit and its power supply, shown in Figure (3-3). This unit synchronizes the flashlamp trigger with the rotating prism, so that the Q of the oscillator is switched on only when the laser rod has been pumped to its maximum population inversion.

FIGURE (3-2)

Photograph of the GNB laser energy subsystem. The device resting on the top of the housing is an error meter, which can be used to precisely control the charging of the capacitor banks. The switch protruding from the same surface controls the relay connecting the two sets of capacitor banks.

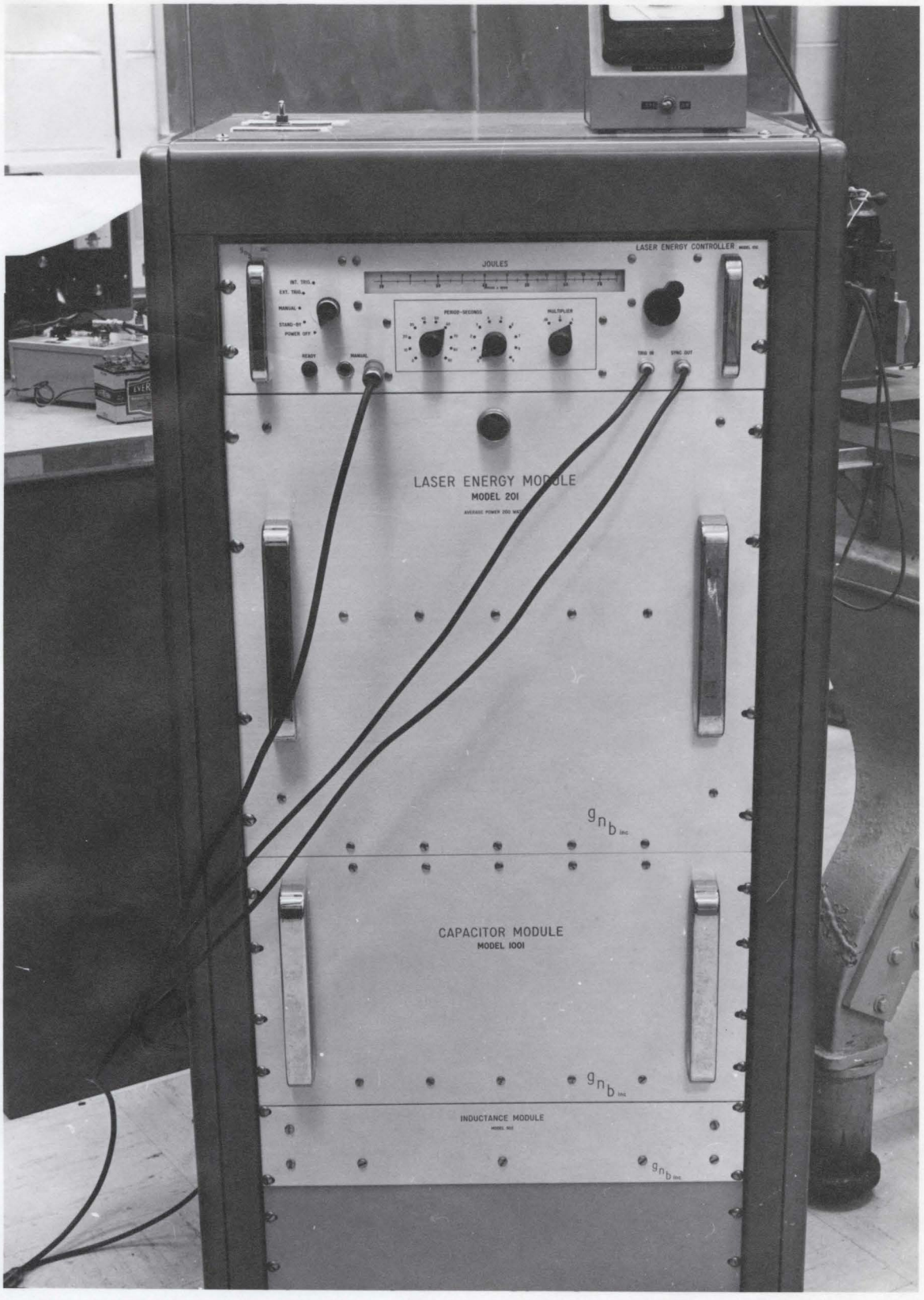
LASER ENERGY CONTROLLER
JOULES
INT. TRIG.
EXT. TRIG.
MANUAL
STAND-BY
POWER OFF
READY
MANUAL
PERIOD-SECONDS
MULTIPLIER
TRIG IN
SYNC OUT
LASER ENERGY MODULE
MODEL 201
gnb inc
CAPACITOR MODULE
MODEL 1001
gnb inc
INDUCTANCE MODULE
gnb inc

FIGURE (3-3)

Photograph of the synchronizing unit, which synchronizes the flashlamp pulses with the rotating prism Q-spoiler.

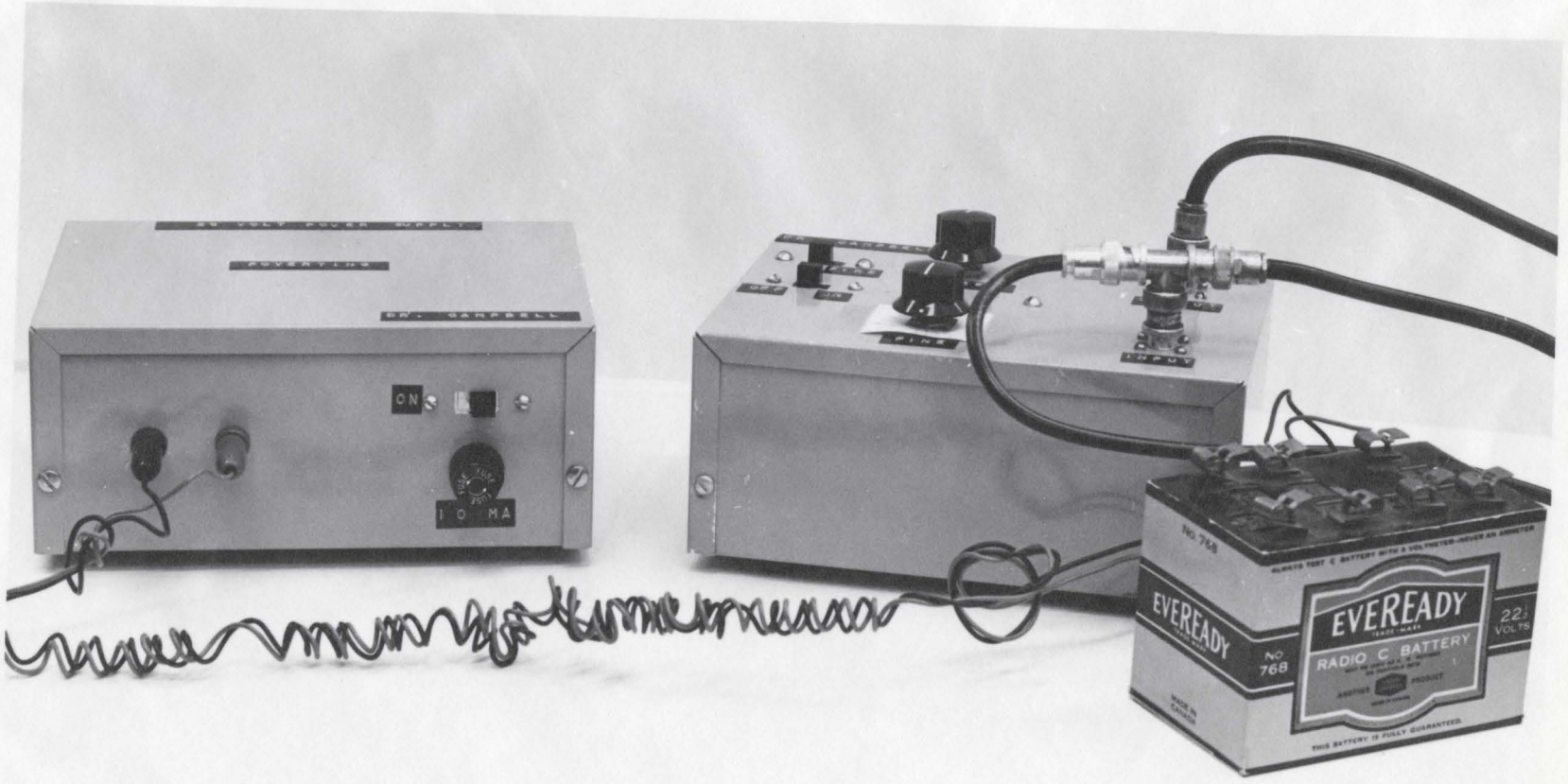
ON
10 MA
EVEREADY
RADIO C BATTERY
NO 768
22½ VOLTS

The T-connector in Figure (3-3) allows us to feed the pickup coil signal to a frequency counter as well, so that we can observe the prism rotational rate at any time.

Third, and last, there is the subsystem concerned with detection. This includes a microvoltmeter (TRG Model 102) connected to the TRG detector mentioned in the previous section, which measures the total energy in the pulse. Also, it includes the fast photodiodes and their backbiasing circuitry, which are used to convert the photon pulse amplitude into voltage, displayable on an oscilloscope.

Each of these three subsystems is described in detail in the following subsections.

3.2.1 The GNB Laser Energy Subsystem -

The GNB laser energy subsystem consists of four modules. The Controller Module, as the name suggests, includes the controls governing the Energy Module. The Energy Module consists of the circuitry for charging the eight capacitors banks, four of which are located in the Energy Module, and four of which are housed in a separate Capacitor Module. The Energy Module is used to charge these banks to any value between 1100 and 2200 volts. Two large coils comprise the fourth module, called the Inductance Module. These coils are used as current limiting chokes.

All connections between the capacitor banks of the Energy Module, those of the Capacitor Module, and the coils of the Inductance Module, are made externally to the modules, but internally to the GNB housing shown in Figure (3-2). This arrangement makes it fairly simple to connect the

capacitor banks in the Energy Module with those in the Capacitor Module by means of a relay. This relay makes it possible to charge the banks supplying power to the amplifier flashtube, independently of the banks supplying power to the oscillator flashtube. This circuit is shown in Figure (3-4), as part of the laser energy subsystem.

The Controller Module also controls the trigger generator, which produces the 20,000 volt trigger to fire the flashtube. In this experiment, the triggering control was left in the "External Trigger" mode. This made it possible to control the triggering by means of the synchronizing subsystem, as indicated in Figure (3-4).

3.2.2 The Synchronizing Subsystem -

This subsystem consists of the pickup coil, the synchronizing unit and its power supply as shown in Figure (3-3), and a frequency counter. The synchronizing unit produces a 10+ volt pulse which sets off the 20,000 volt GNB flashtube trigger, so that the flashtubes are fired at a fixed phase of the sine wave from the rotating prism pickup coil. The unit does this by first clipping and amplifying the 0.5 - 2.5 volt sine wave, squaring by means of an adjustable Schmitt trigger, and then differentiating. It then uses the negative-going spikes of the resulting pulse train to fire a unijunction transistor. It is this unijunction transistor which provides the required 10+ volt pulses. Figure (3-5) shows the schematic of the synchronizing unit, as part of the synchronizing subsystem.

The prism position at which the 10+ volt pulse occurs can be

FIGURE 3-4)

The GNB laser energy subsystem, showing the relation of the synchronizing subsystem.

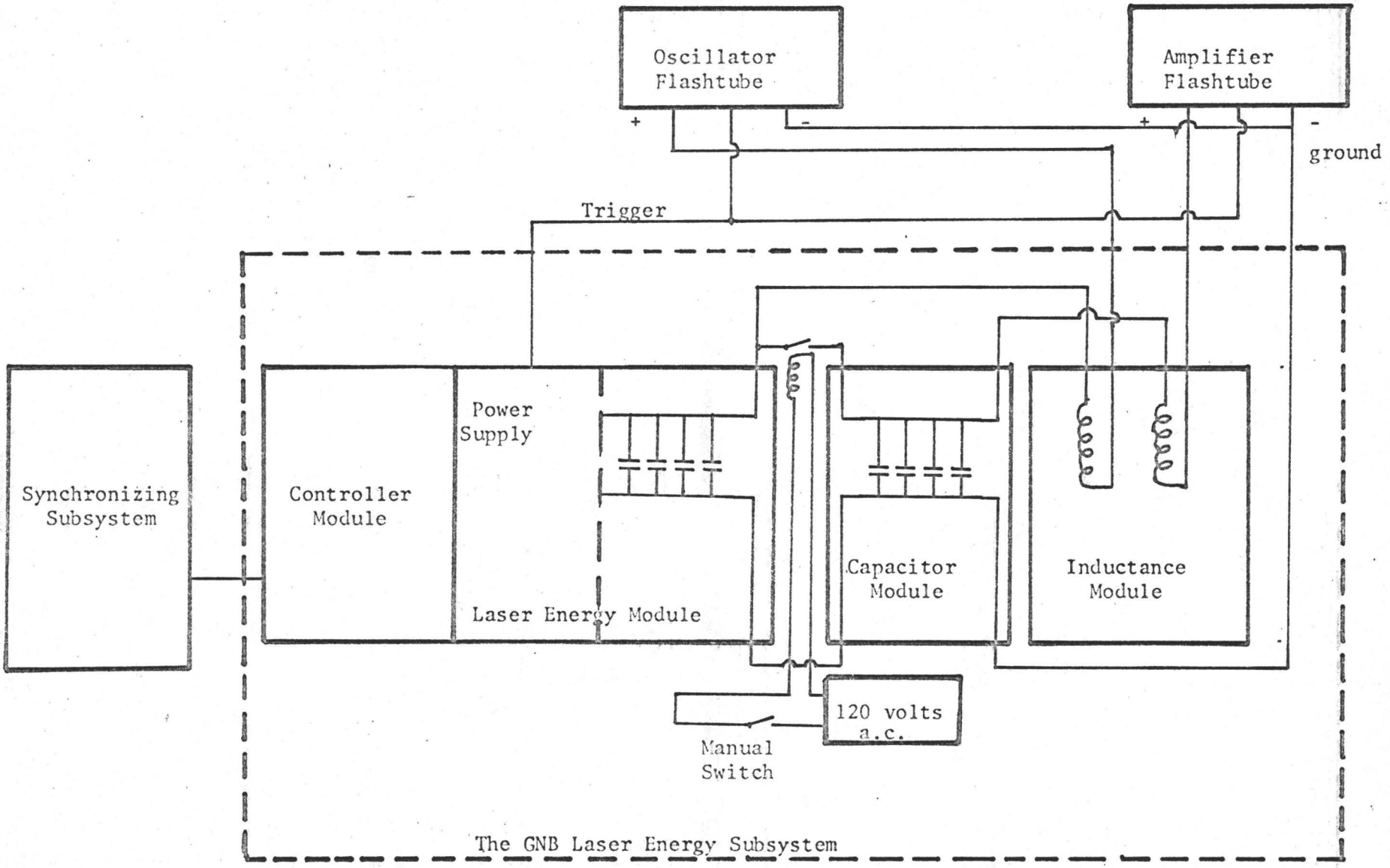
Oscillator Flashtube
Amplifier Flashtube
+
-
+
-
ground
Trigger
Synchronizing Subsystem
Controller Module
Power Supply
Laser Energy Module
Capacitor Module
Inductance Module
120 volts a.c.
Manual Switch
The GNB Laser Energy Subsystem

FIGURE (3-5)

The synchronizing subsystem, showing the schematic for the synchronizing unit.

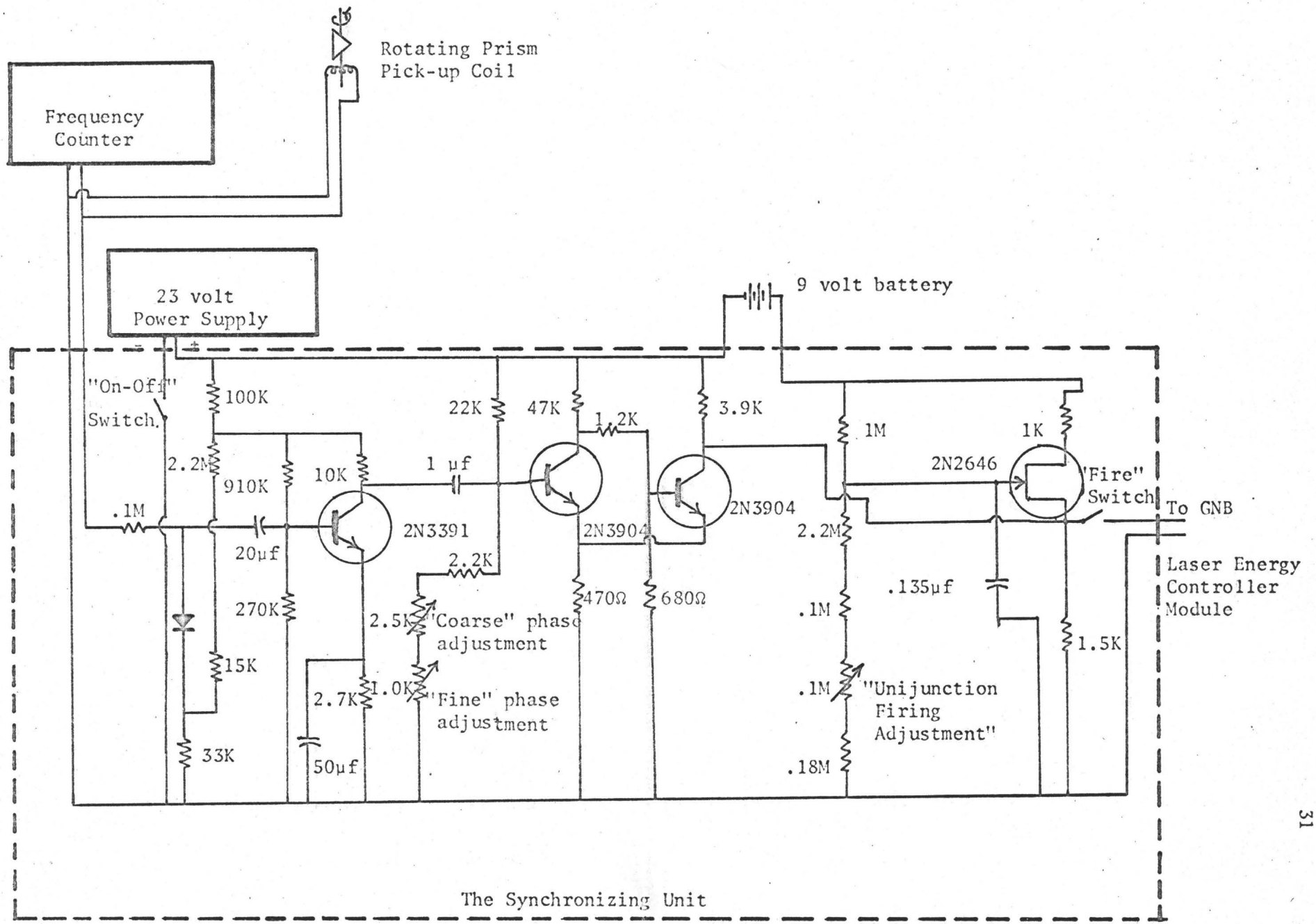
Rotating Prism
Pick-up Coil
Frequency Counter
23 volt Power Supply
9 volt battery
"On-Off" Switch
100K
2.2M
910K
.1M
20µf
10K
2N3391
1 µf
22K
47K
1.2K
2N3904
2N3904
3.9K
2N3904
2.2K
2.5K
"Coarse" phase adjustment
1.0K
"Fine" phase adjustment
2.7K
50µf
270K
15K
33K
470Ω
680Ω
1M
2.2M
.1M
.1M
.18M
"Unijunction Firing Adjustment"
1K
2N2646
"Fire" Switch
To GNB
.135µf
1.5K
Laser Energy Controller Module
The Synchronizing Unit

crudely varied over 360 degrees, by loosening the top of the prism housing, and rotating the pickup coil with respect to the prism. The potentiometer controlling the Schmitt trigger (the FINE control in Figure (3-3)) can then be used as a trimmer, varying the phase at which the 10+ volt pulse occurs, over about 10 degrees.

Since the delay between the triggering of the flashtubes, and the Q-switching of the prism, will vary with prism rotational speed, this must be kept constant by continual adjustment of the air pressure. The frequency counter is used to indicate what adjustments must be made.

We now see that this subsystem allows us to obtain the delay, which yields maximum pumping of the laser rods when the prism is Q-switched. In practice, this optimum delay is about 400 microseconds.

3.2.3 The Detection Subsystem -

This subsystem consists of several units. First, there is the TRG Model 102 Energy Meter, which is the microvoltmeter connected to the TRG Model 101 Ballistic Thermopile. The Energy Meter is calibrated in joules, so that the maximum joule reading, observed one or two seconds after the laser is fired, is the total energy in the pulse. From Figure (3-1), we can see that this is the pulse energy after it has passed through the amplifier rod.

The photodiode which detects the pulses after deflection by the beam splitter in front of the input cone of the Ballistic Thermopile, is connected to Channel 1 of the oscilloscope. The connection is made by means of 30 meters of BNC cable, which provides a delay of 120 nano-

seconds. A second photodiode, an EG&G SGD-100, is connected by 1 1/2 meters of BNC cable to Channel 2 of the oscilloscope. This second photodiode is positioned to receive that part of the beam which is reflected from the beam splitter, i.e., it sees the pulse before it is amplified. The oscilloscope, a Tektronix Model 454, is left in the "add" mode. This allows us to see both the unamplified pulse, and, 80 nanoseconds later, the amplified pulse, in the same oscillogram.

It is important, in connecting these photodiodes to the oscilloscope, to terminate the BNC cables in their characteristic impedances. This enables us to eliminate ringing in the cables, and to transmit the pulse shape to the oscilloscope without distortion. Now, since we also know that the rise-times of the photodiodes are four nanoseconds or less, and that the rise-time of the oscilloscope is less than three nanoseconds, we can conclude that the pulse shapes observed in the oscillograms are a good approximation to those which actually occur.

In order to trigger the 200 nanosecond (20 nanosecond/division) sweep of the oscilloscope at the proper time, two stratagems are employed. First, the A Sweep is triggered form the "SYNC OUT" of the GNB Controller Module. The B Sweep is held off for the first 300 microseconds of the A Sweep by leaving the B triggering switch in the "B triggerable after delay time" position. This stratagem circumvents the difficulty that otherwise, noise from the flashtube trigger pulse triggers the B sweep too early. The second stratagem is to trigger the B sweep off the photon beam itself, by means of a second beam splitter and a fairly fast phototube. This is, in fact, the only way this triggering could be done, since

any other method would require a delay time accurate to within 0.01%.

The entire detection subystem is shown in Figure (3-6).

3.3 Procedures:

The alignment procedure, as mentioned earlier, consists primarily of aligning each part by means of the autocollimator. It is, however, necessary to use a low-power He-Ne laser for alignment in several instances. First, the light from the autocollimator source, reflected from the laser rod end faces, is insufficient to be seen with the autocollimator telescope. Consequently, the He-Ne laser is used to align the rods parallel to the output reflector normal, to within a minute or so of arc. Second, in the case where a Brewster angle rod is used, the autocollimator principle is invalid, again necessitating the use of the He-Ne laser. Finally, it is also necessary to use the He-Ne laser to position the various detectors.

The procedure for charging the oscillator flashtube storage capacitors, independently of the amplifier flashtube storage capacitors, is quite simple. First, the relay connecting the two sets of banks is closed, and the combined capacitance is charged to the voltage desired for the amplifier flashtube storage capacitors. Next, the relay is opened, leaving only the oscillator flashtube storage capacitors still connected to the Energy Module. These capacitors are then charged to the value desired for the oscillator, after which the flashtubes are triggered. It is a good assumption that the leakage from the amplifier flashtube storage capacitors, which occurs in the time taken to charge the oscillator flashtube storage capacitors, is negligible.

FIGURE (3-6)

The detection subsystem.

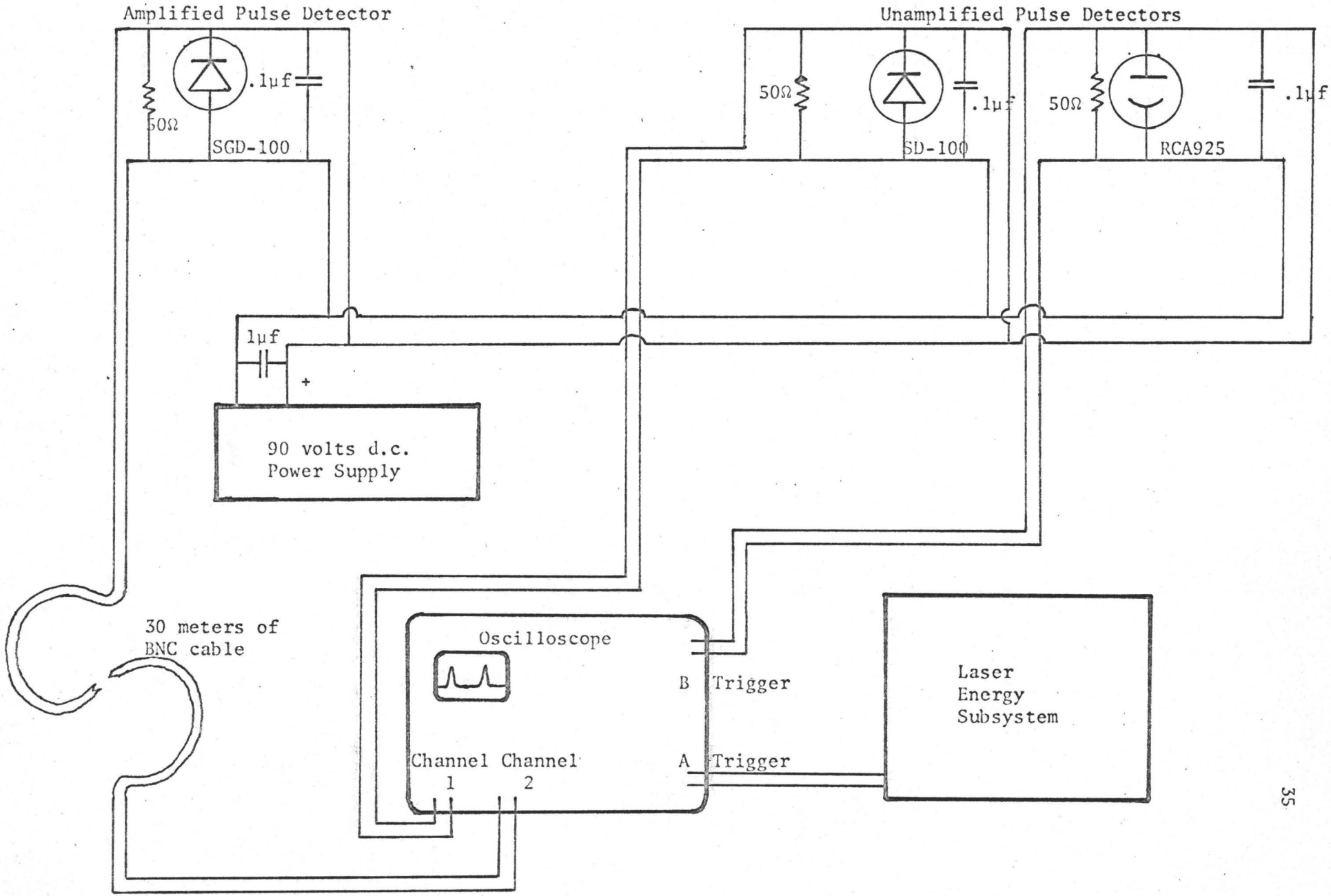
Amplified Pulse Detector
.1μf
50Ω
SGD-100
Unamplified Pulse Detectors
50Ω
.1μf
SD-100
50Ω
RCA925
.1μf
1μf
+
90 volts d.c.
Power Supply
30 meters of
BNC cable
Oscilloscope
B Trigger
A Trigger
Channel 1
Channel 2
Laser
Energy
Subsystem

In the procedure of the experiment itself, measurements of energy gain are made before those of power gain. Since the theoretical calculation of energy gain at saturation is simple (Section 2.5), whereas that for power gain is not, this procedure allows us to ensure that the amplifier is not saturating before proceding further. The actual procedures for making the energy gain and power gain measurements are given in subsections 3.3.2 and 3.3.3, following a subsection on amplifier pump energy determination.

3.3.1 Procedure for Determining Amplifier Pump Energy -

The amplifier pump energy E, as used in the calculation for population inversion (Section 2.6), can be non-linear with the electrical energy input to flashlamp for two reasons. First, since the electrical energy is varied by changing the voltage on the capacitors, and since the flashtubes operate differently at different voltages, the light energy output of a flashtube may not be linear with the electrical energy input. Second, the fact that the upper laser level lifetime is finite implies that only a certain fraction of the light energy reaching the rod is effective, i.e., the ions pumped by the remaining fraction decay before the arrival of the laser pulse. Thus, since the flashlamp output pulse shape varies with the input power, a further non-linearity may be introduced.

Determination of the non-linearity, in order to correct for it, is carried out as follows. First, oscillograms are taken of the flashlamp pulse as a function of time. The SGD-100 photodiode, which conveniently

has a good spectral response in the region of the pumping radiation, is used for this purpose. The output of the photodiode circuit is a linear function of power, i.e., the sensitivity is a constant $\approx$ 0.5 microamperes/microwatt, so that the oscillogram height above the base level is a direct measure of power, and hence of pumping radiation incident on the rod.

These pumping flash oscillograms, roughly 360 μseconds in length, are now divided up into increments of 20 μseconds each. The height of each increment is measured, and is multiplied by $\exp(-\frac{\ln 2}{.000360} t)$ to correct for the finite upper laser level lifetime. (The quantity t is the time in seconds from the increment to the arrival of the laser pulse.) The sum of the increments, each multipled by this factor, now gives us a measure of the amplifier pump energy E, with the two sources of non-linearity removed. This amplifier pump energy is then plotted against the corresponding electrical energy input to the flashlamp. The resulting curve gives us a means of easily determining the amplifier pump energy, since electrical energy input can be read from the laser energy controller module.

3.3.2 Procedure for Measuring Energy Gain -

As described earlier, the oscillogram obtained from each firing of the laser contains first, the laser pulse output of the oscillator, and 120 nanoseconds later, this same pulse after it has passed through the laser amplifier rod. The first step in measuring gain is to relate the height of the first pulse in the oscillogram to the energy of the pulse before amplification. This is done by plotting the variation in the height of the first pulse, against the variation in the energy

measured by the ballistic thermopile, when the amplifier rod is left unpumped. Energy gain measurements follow immediately when the amplifier rod is pumped, since the ballistic thermopile gives the amplifier output and the height of the first pulse now gives the amplifier input.

The next step is to measure the energy gain for an input pulse about an order of magnitude smaller, to determine whether saturation is occurring. This reduction is accomplished by placing a thin filter of $CuSO_4$ solution just before the laser amplifier. Since the resultant amplified pulse is too small to measure accurately by means of the ballistic thermopile, the second pulse on the oscillogram must be used for this measurement. As noted in the preceding subsection, the height of the oscillogram above the base level is a linear function of power. This means that the area of this second pulse will be linearly related to the energy of the pulse after amplification. To find the slope of this line, we begin by measuring the areas of second pulses in the oscillograms taken for the preceding energy gain measurements. These areas, plotted against the energies recorded from the ballistic thermopile, give a straight line of measureable slope. The attenuating $CuSO_4$ filter is now put in place, and the sensitivity of channel one of the oscilloscope, to which the amplified pulse detector is connected, is increased until a good oscillogram of the amplified pulse is obtained. Several oscillograms are now taken with the amplifier unpumped. The areas of the second pulses of these oscillograms, divided by the increase in oscilloscope sensitivity, give us the $CuSO_4$-attenuated laser pulse energies, by means of the straight line relation just obtained. Since the height of the first pulse gives

us the laser pulse energy before attenuation, the attenuation factor is obtained. Energy gain measurements follow immediately when the amplifier rod is pumped.

As a final check on the results, the input pulse energy is now reduced by another order of magnitude, by means of a much thicker $CuSO_4$ filter. Before replacing the thin filter with the thick one, it is first necessary to remove some of the protective cardboard filter from in front of the amplified pulse detector. The oscilloscope sensitivity is then reduced to something like its original value, so that a reasonalbe pulse amplitude occurs on the oscillogram. Several oscillograms are taken, with the amplifier rod umpumped, to obtain the new pulse area versus energy relation. The thick $CuSO_4$ filter then replaces the thin one, the sensitivity of the oscilloscope is increased, and more oscillograms are taken with the amplifier unpumped. From these oscillograms, the new attenuation factor is obtained, in the same manner as was the first attenuation factor. The amplifier is now pumped, and the final measurements of energy gain are made.

Some minor variations in the procedure of this section, due only to a lack of previous experience with the apparatus, were made. Since these variations concern only questions of chronological order and repeats of measurements, however, they are not discussed here, but are left for the reader whose interest leads him to a careful perusal of the data presented in Appendix III.

3.3.3 Power Gain Measurement Procedure -

It was hoped that the oscillograms used to obtain the energy gain measurements would be able to furnish power gain measurements as well. Theoretically, this should be quite simple; since the area of the pulse in the oscillogram is the integral of the height, which is directly proportional to the power, we have:

$$\text{area} = \int \text{height } dt = \int \text{constant x power } dt$$

$$= \text{constant x energy}$$

and so,

$$\text{power} = \frac{\text{energy}}{\text{area}} \text{ x height.}$$

However, as will be explained in the chapter containing the results, this was not possible in our case. Even if it were possible, however, it is highly unlikely that any new information would come to light, since in the development of the theory, the calculation of energy gain follows, and is based on, the calculation of power gain.

CHAPTER IV

EXPERIMENTAL RESULTS

4.1 Relation of Amplifier Pump Energy to Electrical Energy Input to Flashlamp:

This relation was obtained by the method outlined in the procedure; the resultant curve is given in Figure (4-1). This curve is broken into three parts corresponding to three different storage capacitor arrangements. In the lowest range, only one capacitor is used, with the result that the flashlamp pulse shape is shortened. Thus, in this range, the flashlamp pulse has finished eighty microseconds before the arrival of the laser pulse. In the centre range, three capacitors are used, with the result that the pulse shape is longer, so that the end of the flashlamp pulse and the arrival of the laser pulse are nearly simultaneous. In the highest range, with four capacitors, the pulse shape is lengthened further, so that the laser pulse arrives approximately eighty microseconds before the end of the flashlamp pulse. It is these differences in pulse shape, together with the fixed time of arrival of the laser pulse, which give rise to the discontinuities in the curve.

4.2 Energy Gain Results:

A typical set of five oscillograms, from which these energy gain measurements were made, is shown in Figure (4-2). As described in the preceding chapter, the first pulse in each oscillogram gives the time development of the pulse input to the amplifier, and the second pulse

FIGURE (4-1)

Relation of the amplifier pump energy, E, to the electrical energy input to the flashlamp.

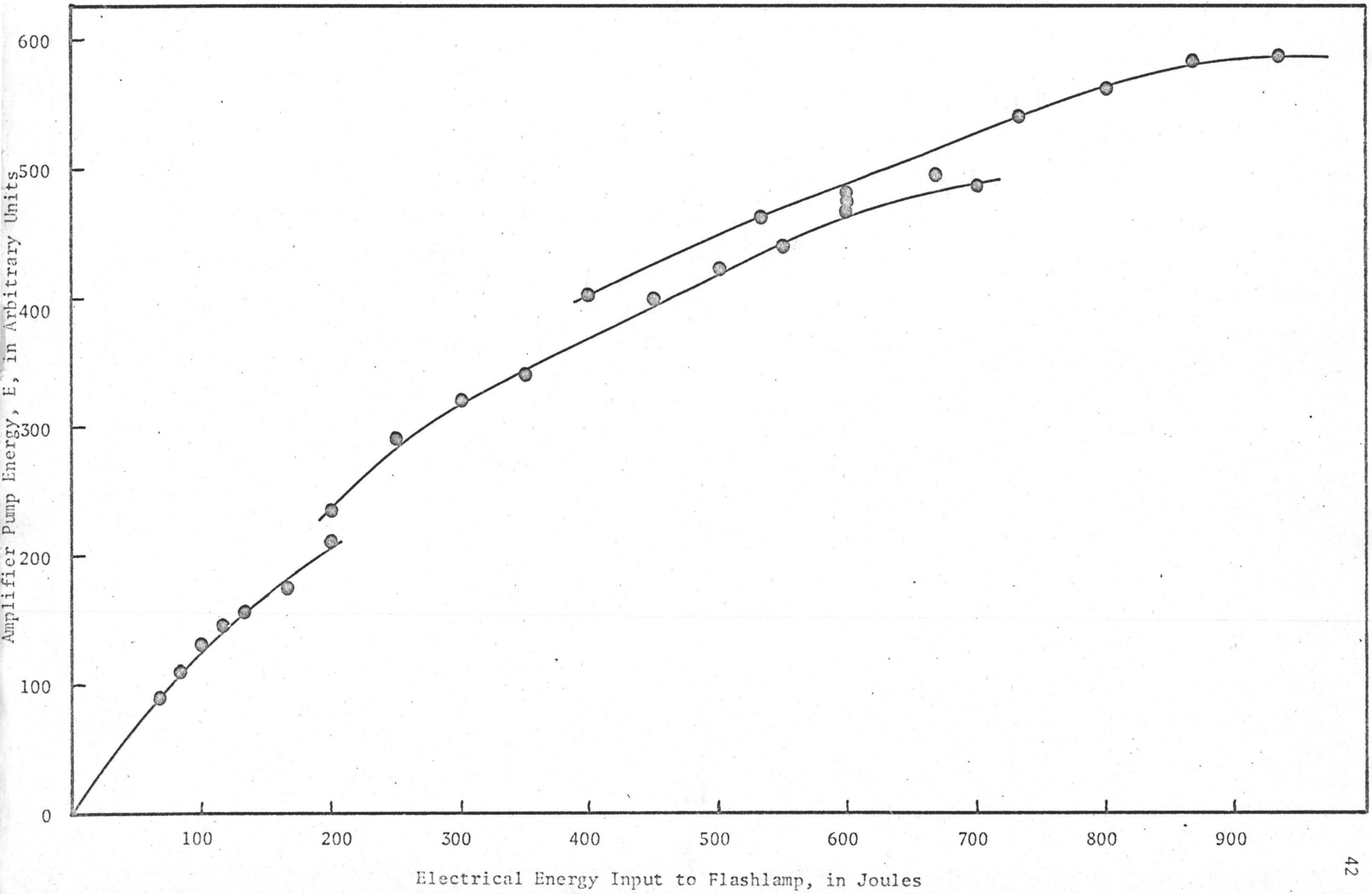
600
500
400
300
200
100
0
Amplifier Pump Energy, E, in Arbitrary Units
100
200
300
400
500
600
700
800
900
Electrical Energy Input to Flashlamp, in Joules

FIGURE (4-2)

A typical set of five oscillograms, from which energy gain measurements were made. The time scale is 20 nanoseconds per division. The pumping of the amplifier in each case was (in arbitrary units):

(a) 0

(b) 240

(c) 370

(d) 468

(e) 492

(a)

(b)

(c)

(d)

(e)

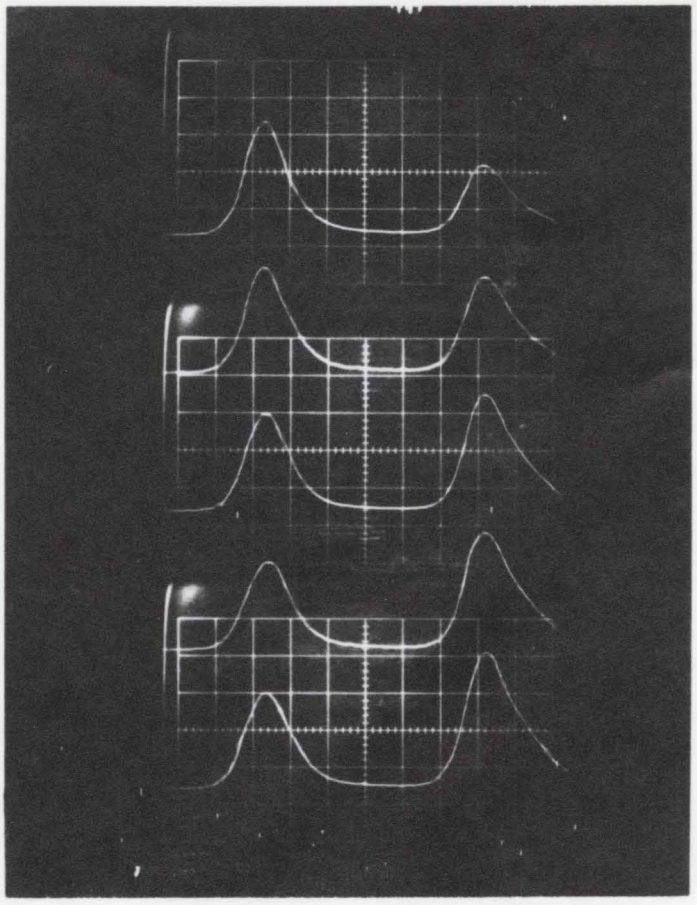

gives the time development of the same pulse as it emerges from the amplifier. As can be seen from this photograph, the pulse is stretched out slightly as it emerges from the amplifier. Since this occurs even in the case in which the amplifier is unpumped, we see that this stretching out is due, not to any nonlinear gain effect of the amplifier, but rather to the unavoidable capacitance of the BNC cable used to delay the signal from the second photodiode. This stretching out, fortunately, is sufficiently slight so that it does not observably affect the following energy gain measurements.

These measurements begin with the determination of the experimental relation of the unamplified pulse energy to the height of the first pulses in the oscillograms. The result of this determination is given in Figure (4-3). No significance attaches to the curve itself; as mentioned in the procedure, it is merely a convenient method for determining the pulse energy output of the laser oscillator. The output from the laser amplifier is measured directly with the ballistic thermopile; the resultant gain of the amplifier is displayed in Figure (4-4). This graph displays the data in condensed form, i.e., each point on this graph is the average of nine or more experimental points. The smooth curve shown is fitted to the experimental points by the method of least squares, using the model demanded by the theory of Chapter II, for the case in which saturation does not occur. This model is:

$$G_E = \frac{1}{1 - [1 - e^{-\sigma N_o L}][1 - (K_1+K_2)\frac{\sigma D}{2}]} \approx e^{\sigma N_o L} = e^{\sigma L \times .30 N_{go}(1-e^{-\gamma E})}$$

FIGURE (4-3)

Experimental relation of the unamplified pulse energies to the heights of the corresponding pulses in the oscillograms.

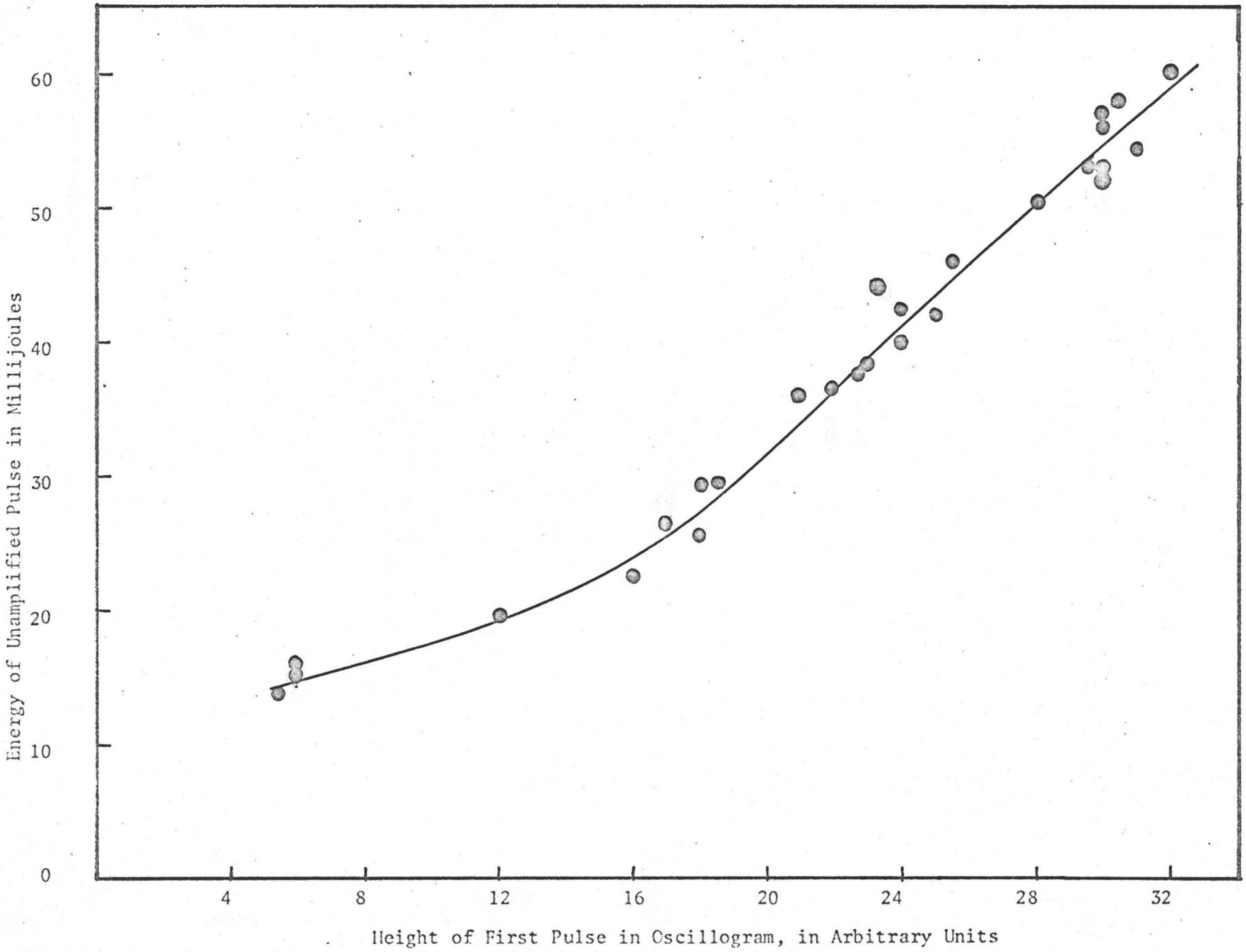
Energy of Unamplified Pulse in Millijoules
0
10
20
30
40
50
60
4
8
12
16
20
24
28
32
Height of First Pulse in Oscillogram, in Arbitrary Units

FIGURE (4-4)

Energy gain of the laser amplifier, for input pulses of 20-50 millijoules total energy. The points are averages of nine or more experimental points. The smooth curve has the shape given by the theory. It is determined by the method of least squares, from the uncondensed experimental points.

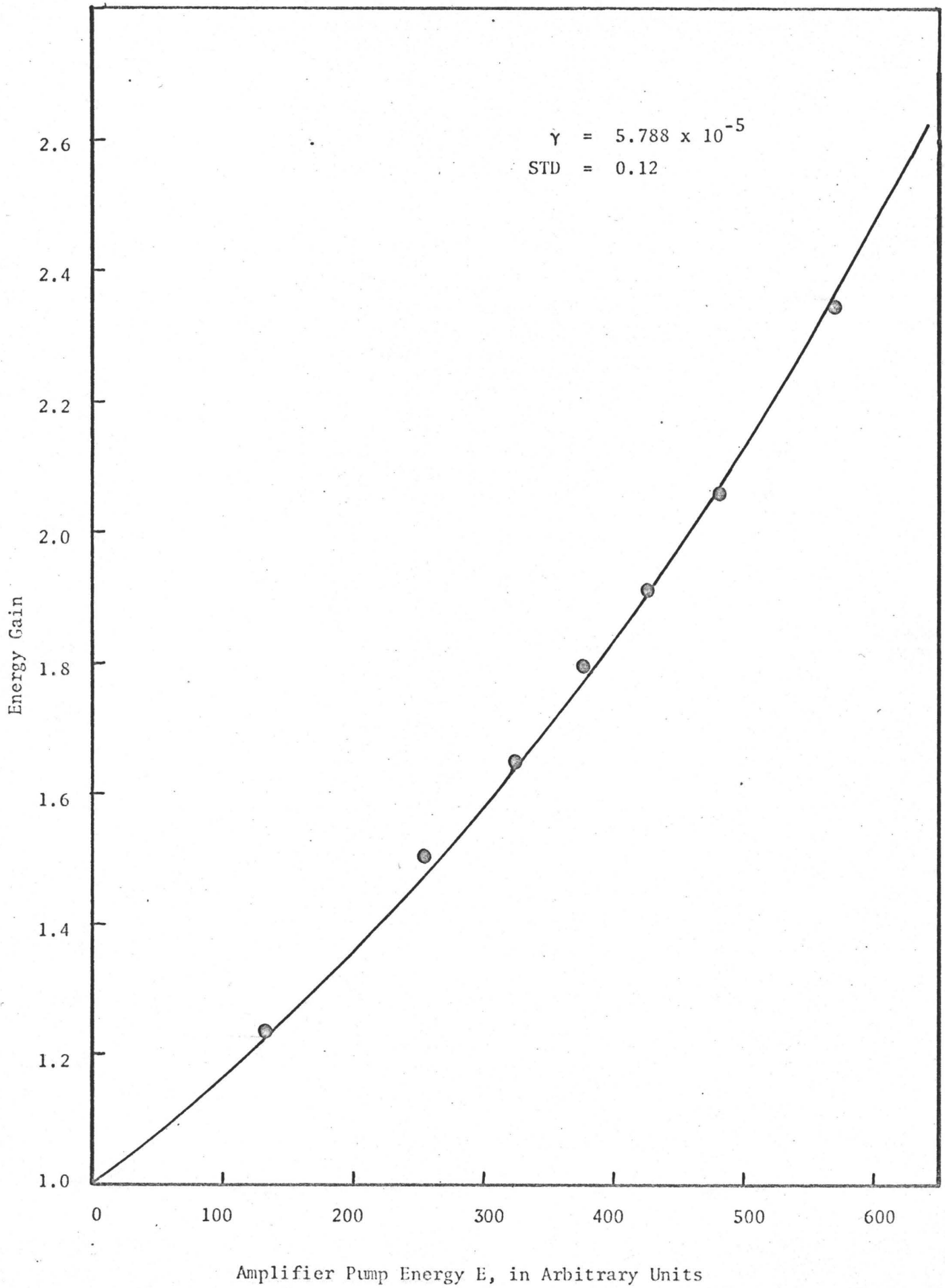
γ = 5.788 x 10^-5
STD = 0.12
Energy Gain
2.6
2.4
2.2
2.0
1.8
1.6
1.4
1.2
1.0
0
100
200
300
400
500
600
Amplifier Pump Energy E, in Arbitrary Units

The factor $[1 - (K_1 + K_2)\frac{\sigma D}{2}]$ is neglected, since for the largest input pulse energy used, namely 50 millijoules, we have $D = 6.15 \times 10^{17}$ photons/cm^2. And since Hill[6] estimates $K_1 = 0.13$, and $K_2 = 0.314$, and since Cabezas, McAllister, and Ng[3] find $\sigma = 3.5 \times 10^{-20}$ cm^2, we find that this factor is nearly equal to one, i.e., $[1 - (K_1 + K_2)\frac{\sigma D}{2}] = 0.995 \simeq 1.00$.

Since we know both the quantity L(7.61 cm.) and the quantity $N_{go}(3.3 \times 10^{20}/cm^3)$ from the data supplied by Kodak for the doped rod, the only unknown in the model is γ. It is this parameter which is varied to minimize the residual sum of squares. The standard deviation given on the graph is that of the unaveraged experimental points from the fitted curve; it is a measure of the scatter of the eight-six experimental points.

We observe from the graph that all of the condensed points are remarkably close to the fitted curve, i.e., the curve shape given by the theory appears to be in agreement with the experimental results. Thus, it appears that the amplifier is not saturating; saturation, as shown in the theory, would give a straight line relation. For a verification of this, however, the gain measurements for attenuated input pulses were carried out. If saturation were occurring, greater gains should be observed for the attenuated input pulses.

Before these measurements could proceed, however, a minor readjustment of the unamplified pulse detector necessitated a new determination of the relation between the unamplified pulse energy and the height of the first pulse in the oscillogram. The new experimental relation is given in Figure (4.5).

FIGURE (4-5)

The second experimental relation of the unamplified pulse energies to the heights of the corresponding pulses in the oscillograms.

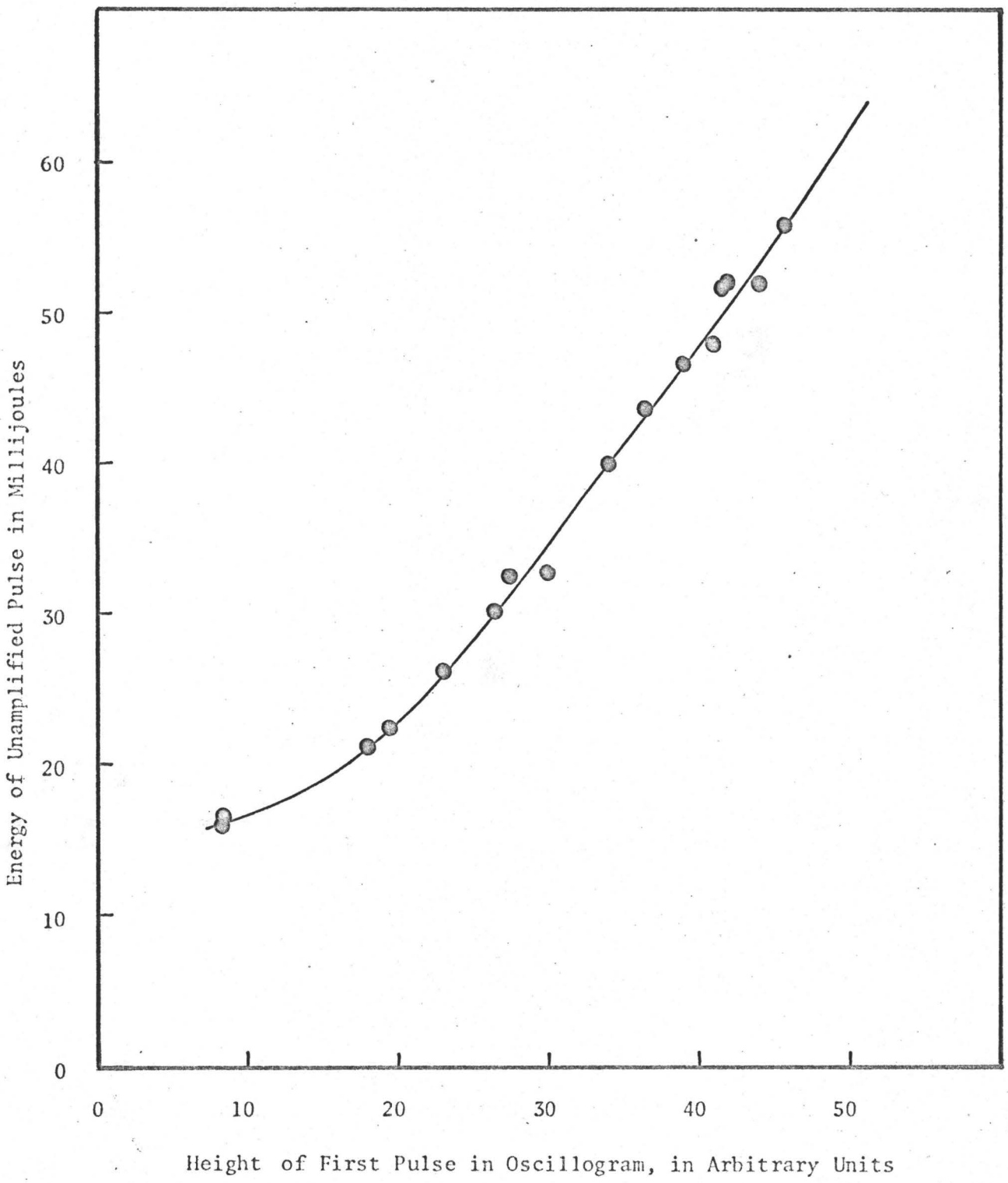
Energy of Unamplified Pulse in Millijoules
0
10
20
30
40
50
60
0
10
20
30
40
50
Height of First Pulse in Oscillogram, in Arbitrary Units

The next step, as mentioned in the procedure, was to find the relation between the area of the second pulse in the oscillogram, and the output pulse energy. This is given in Figure (4-6).

At this point, the $CuSO_4$ filter was put in place. The oscilloscope sensitivity for the amplified pulse detector was increased by a factor of ten, in order to see the amplified pulse. The slope of the relation of Figure (4-6) was divided by a factor of ten, to give the output energy from the amplifier. This energy, obtained with the amplifier rod unpumped, is then compared with the energy output of the oscillator, given by Figure (4-5). This yields the attenuation factor of the $CuSO_4$ filter, 0.0379. The amplifier is now pumped to obtain the required gain measurements. The results are displayed in Figure (4-7). This Figure is set up exactly as was Figure (4-4), except that the condensed points are averages of four or more, rather than nine or more, experimental points.

We observe from Figure (4-7) that the energy gains observed are nearly the same as for the unattenuated input pulses (Figure (4-4)). This confirms our inference from the curve shape of Figure (4-4), that the amplifier is not saturating. The distance of the first condensed point from the theoretical curve in Figure (4-7) may be explained by the fact that it represents an average of only five experimental points, whereas in Figure (4-4), the first condensed point represents an average of nineteen experimental points.

In preparation for a further attenuation of the input pulse, some of the protective cardboard filters were now removed from in front

FIGURE (4-6)

Amplified pulse enrgy, related to the area of the second pulse in the oscillogram. Note that this is a straight line relation.

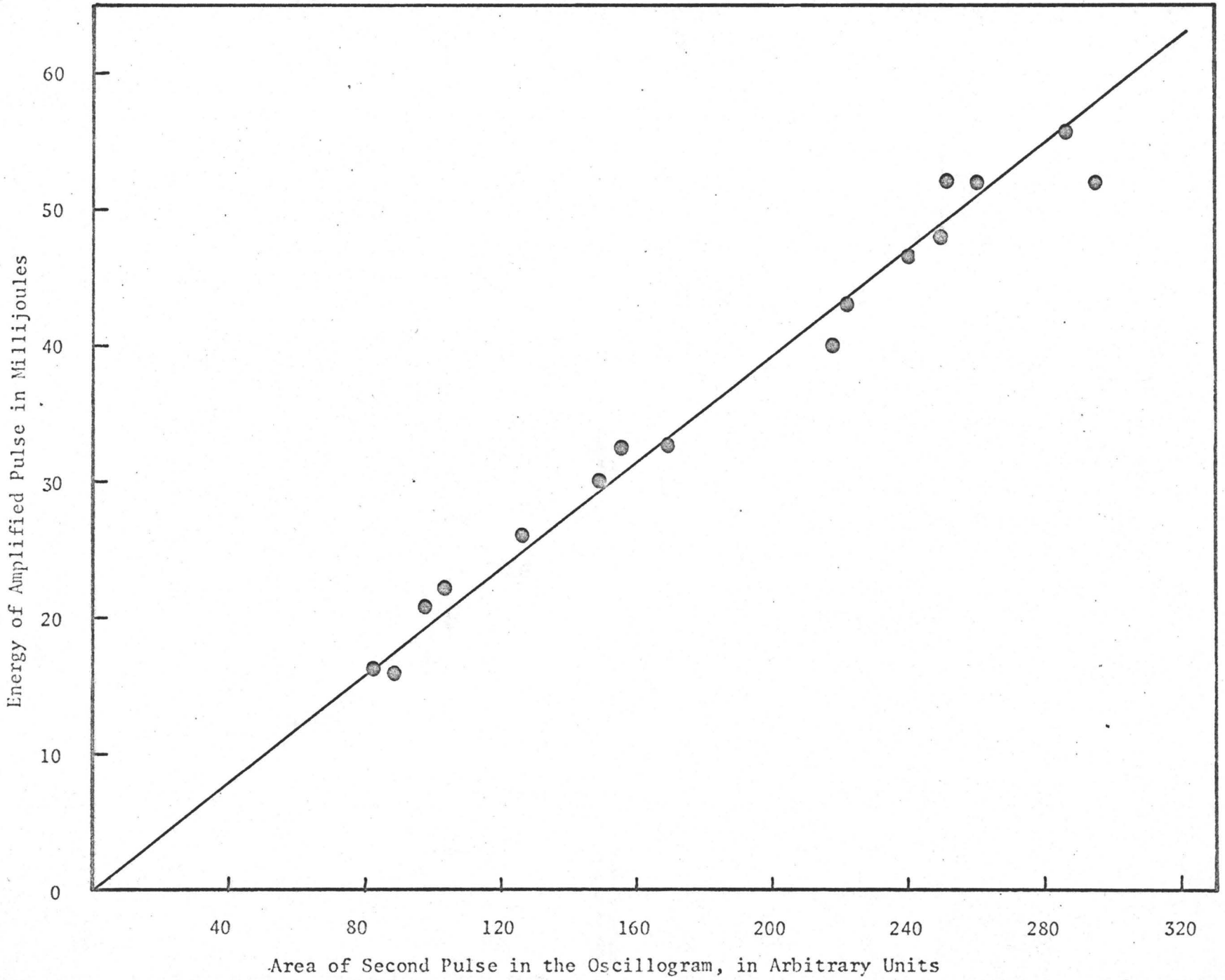

(FIGURE 4-7)

Energy gain of the laser amplifier, for input pulse energies of 0.7-1.4 millijoules. The points are averages of four or more experimental points; as in the previous case, the smooth curve is a least squares fit to the experimental points.

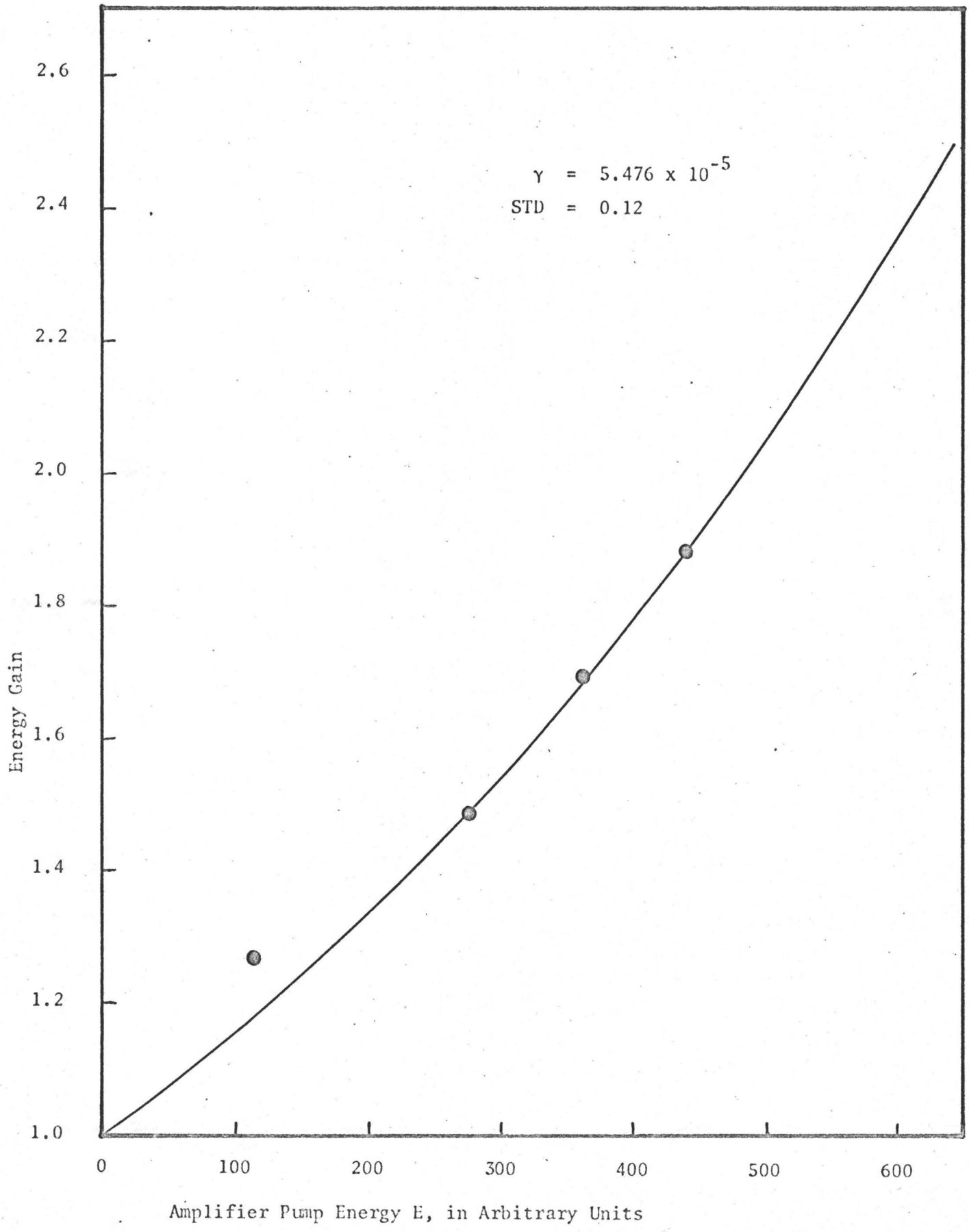
γ = 5.476 x 10^-5
STD = 0.12
Energy Gain
2.6
2.4
2.2
2.0
1.8
1.6
1.4
1.2
1.0
0
100
200
300
400
500
600
Amplifier Pump Energy E, in Arbitrary Units

of the amplified pulse detector, and the oscilloscope sensitivity was decreased. More oscillograms, with the amplifier rod unpumped, were taken. With the first pulses in the oscillograms, and the present attenuation factor, the energies of the pulses were determined. The second pulses in the oscillograms were then used to find the new output pulse area versus energy relation, given in Figure (4-8). The thin $CuSO_4$ filter was then replaced with the thick one, and the oscilloscope sensitivity was increased. In the same manner as before, the attenuation factor was measured, and was found to be 0.00307. The amplifier was now pumped, and the energy gain measurements were made. The results are displayed in Figure (4-9). In this graph, each condensed point is the average of five or more experimental points. In connection with this, we note that the closeness of the condensed experimental points to the theoretical curve is slightly better than in the previous case, in which each condensed point was the average of only four or more experimental points.

As in the previous case, we note that again the energy gains are nearly the same as for the unattenuated input pulses. This reconfirms our statement that the amplifier is not saturating.

4.3 Result of the Attempt to Measure Power Gain:

As could be seen from Section 3.3.3, measurement of power depends directly on the ratio of the pulse height in the oscillogram to its area. This ratio, however, is significantly affected by the "stretching out" observed in Figure (4-2). Consequently, it was impossible to obtain accurate power gain measurements. However, as mentioned in

FIGURE (4-8)

The relation between the amplified pulse energy and the area of the second pulse in the oscillogram, after some of the protective cardboard filters have been removed from in front of the amplified pulse detector.

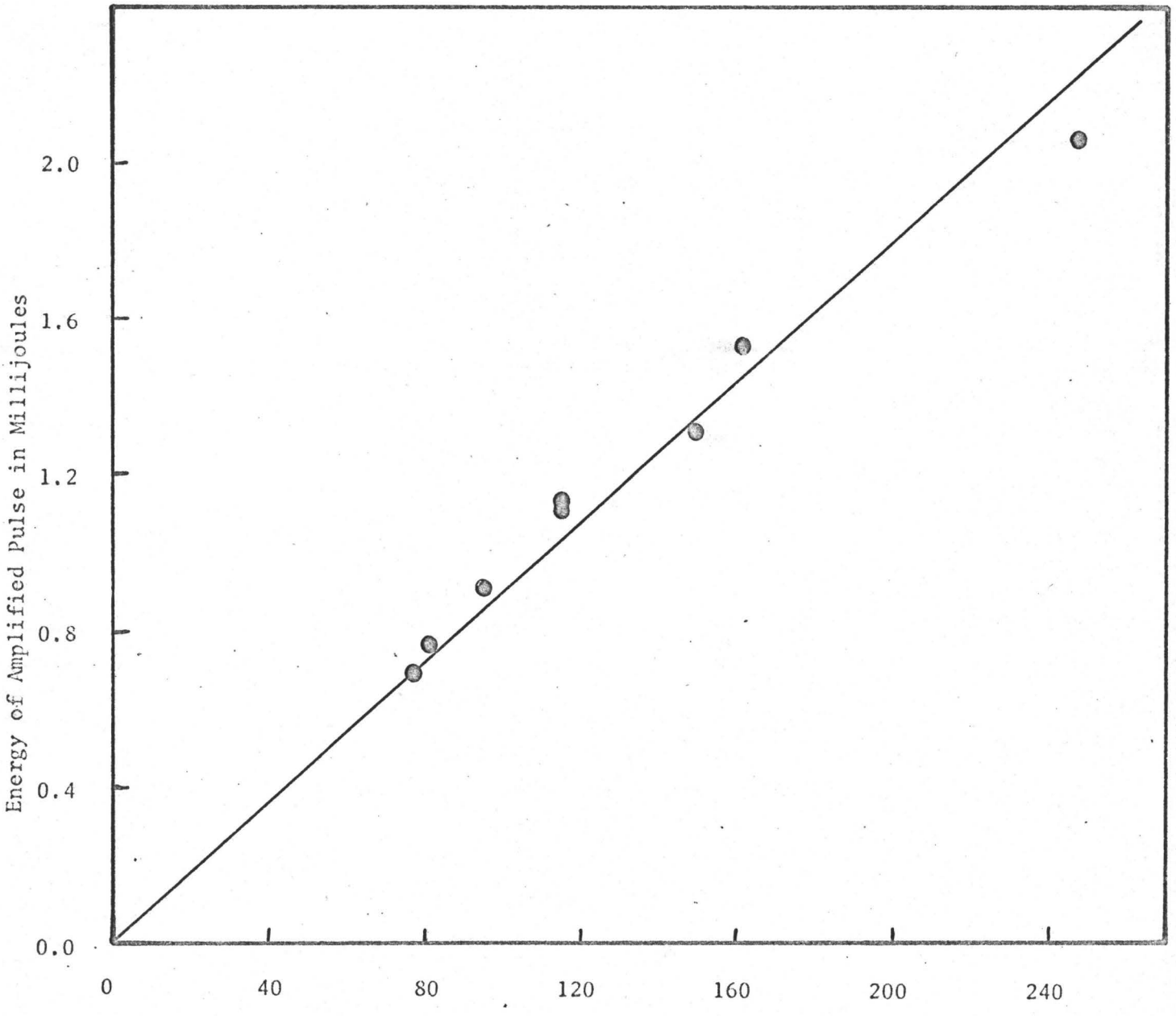
Energy of Amplified Pulse in Millijoules
2.0
1.6
1.2
0.8
0.4
0.0
0
40
80
120
160
200
240
Area of Second Pulse in the Oscillogram, in Arbitrary Units

(FIGURE 4-9)

Energy gain of the laser amplifier, for input pulses of 0.05-0.12 millijoules total energy. The points are averages of five or more experimental points. As in the previous cases, the smooth curve is a least squares fit to the experimental points.

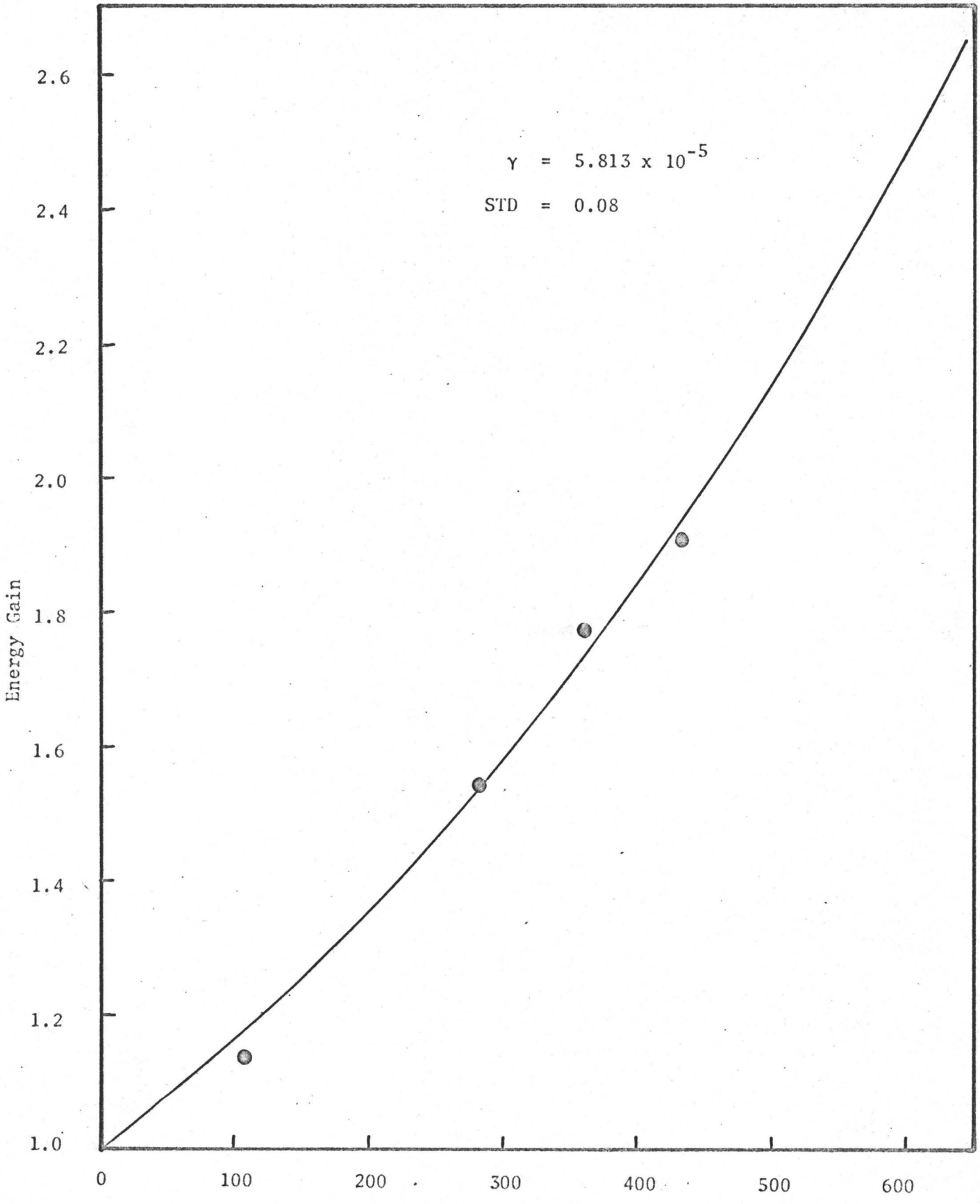
γ = 5.813 x 10^-5
STD = 0.08
Energy Gain
2.6
2.4
2.2
2.0
1.8
1.6
1.4
1.2
1.0
0
100
200
300
400
500
600
Amplifier Pump Energy E, in Arbitrary Units

Section 3.3.3, such measurements are contained in the energy gain measurements, since the theoretical energy gain is derived from the theoretical power gain. Thus, all of the results from which we could desire to draw conclusions have been obtained.

CHAPTER V

CONCLUSIONS

A theory of the four level solid state laser amplifier has been constructed, and applied to the case of the Nd^{3+}-in-glass laser. Experiments were carried out to test this theory, namely, energy gain measurements for a Lorentzian-shaped input pulse. These measurements were made for different pumping energy inputs to the amplifier rod.

Three sets of such measurements were made, the latter two being made with attenuated input pulses. From these latter two, we were able to conclude that the laser amplifier was not saturating. We now consider the first set of results, since it contains over four times as much experimental data as either of the other two, and hence is more reliable for the conclusions to be proposed.

We see from this set, from Figure (4-4), that the relationship demanded by our theory, namely (as shown in Section 4.2):

$$G_E = e^{\sigma L \times 0.30 N_{go}(1 - e^{-\gamma E})},$$

is adhered to rather well. Since this model was fitted to the experimental points by varying the parameter γ, it is now important to test this agreement against variations in other factors, to determine the significance of the agreement.

To this end, in Figure (5-1), we have given with the condensed points the theoretical curve obtained by least squares fit, for various values of σ. σ_{given} is the $\sigma = 3.5 \times 10^{-20}$ cm^2 value found by Cabezas,

(FIGURE 5-1)

Fitted theoretical curves for several values of the stimulated emission cross section σ, compared to the condensed experimental points.

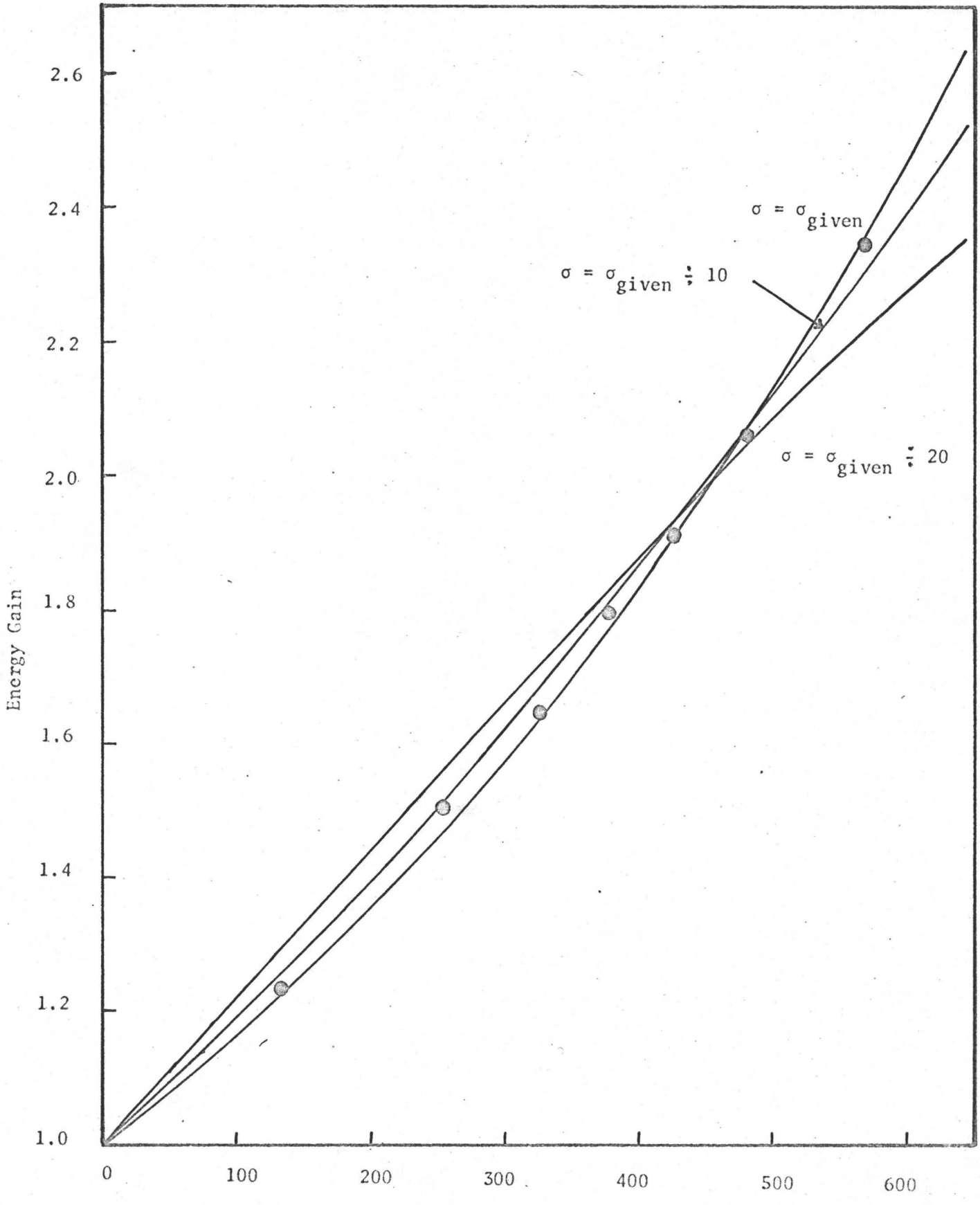
2.6
2.4
2.2
2.0
1.8
1.6
1.4
1.2
1.0
Energy Gain
σ = σ given
σ = σ given ÷ 10
σ = σ given ÷ 20
0
100
200
300
400
500
600
Amplifier Pump Energy E, in arbitrary Units

McAllister, and Ng[3]. A curve for $\sigma >> \sigma_{given}$ (i.e., one for which $e^{\sigma L \times 0.30 N_{go}(1 - e^{-\gamma E})} \rightarrow e^{\sigma L \times 0.30 N_{go} \times \gamma E}$) was also fitted. However, this curve was found to be so close to the curve fitted for $\sigma = \sigma_{given}$, that these were indistinguishable on a graph of the scale shown. Consequently, only the three curves, fitted for $\sigma = \sigma_{given}$, $\sigma = \sigma_{given} \div 10$, and $\sigma = \sigma_{given} \div 20$ appear on this graph.

It is of interest to note that the condensed point lying farthest from the origin, where the three theoretical curves diverge the most, lies on the curve fitted with the value of σ given by McAllister. This suggests that we have evidence to support two conclusions. The first of these is that the true value of σ is not less, within an order of magnitude, than that given by Cabezas, McAllister and Ng. The second conclusion is that our theory is basically correct in the form that it gives for the relation between the amplifier pump energy and the energy gain of the laser amplifier.

We note that it has proved impossible to test that part of the theory which gave rise to the term $[1 - (K_1 + K_2)\frac{\sigma D}{2}]$, since the term was indistinguishable from unity for the values of D which we were able to obtain. This would not be the case, however, for an input pulse, and hence D, an order of magnitude larger than that which was obtainable here. Experiments with an input pulse increased by this amount are recommended to future Nd^{3+}-in-glass laser investigators for the following reason. Hill's[6] estimate of $K_1 = 0.13$ has rather wide uncertainty limits, due to the fact that the distribution of the degeneracies between the two

$^4I_{11/2}$ levels is unknown. The experiment here recommended, if carried out with sufficient accuracy, could be made to furnish a value of K_1 from which the distribution of these degeneracies could be inferred.

It is hoped that these conclusions and recommendations, together with the theory and methods outlined earlier in this thesis, will be of value to those wishing to pursue further the investigation of the Nd^{3+}-in-glass laser amplifier.

APPENDIX I

Justification of the Statement "b << a":

On page 16, we applied the following relationships, namely:

$$a = 1 - [1 - \exp(-\sigma N_o L)]\ [1 - (K_1 + K_2)\frac{\sigma D}{2}\ ]\ , \text{ and}$$

$$b = [1 - \exp(-\sigma N_o L)]\ (K_1 + K_2)\frac{\sigma D}{4}\ .$$

We now list some typical values for the terms in these expressions. These were obtained both from theoretical and experimental work:

$$\exp(-\sigma N_o L) = 0.5$$

$$(K_1 + K_2) = 0.44$$

$$\sigma = 3.5 \times 10^{-20}\ \text{cm}^2$$

$$D = 6.15 \times 10^{17}\ \text{photons/cm}^2$$

These values yield the following results,

$$a = 0.503, \text{ and}$$

$$b = 0.001,$$

which justify the statement on page 16 that b << a.

APPENDIX II

Comparison of $\frac{N_2}{g_2}$ and $\frac{N_4}{g_4}$:

To obtain this comparison, referred to on page 17, we first note that we can obtain a typical value of $N_o = \frac{N_2}{g_2} - \frac{N_4}{g_4}$ from our gain measurements. Thus, the typical value $G_E = 1.7 = e^{\sigma N_o L}$ yields $N_o = 2.1 \times 10^{18}/cm^3$.

Now the level N_4 can be populated in two ways. The first of these is by thermal equilibrium with the ground state. Neglecting degeneracies, we obtain from the Boltmann relation,

$$N_4 = N_{go}\, e^{-\frac{\Delta E}{KT}} = 3.3 \times 10^{20} \exp - \frac{(2000\ cm^{-1} = 4 \times 10^{-13}\ ergs)}{1.38 \times 10^{16}\ ergs/°K \times 300°K}$$

$$= 1.5 \times 10^{16}/cm^3.$$

Since the degeneracy of the N_4 level is at least $2^{(6)}$, we see that at most, $\frac{N_4}{g_4} = 8 \times 10^{15}/cm^3$, from thermal equilibrium.

The second way in which the N_4 level can be populated, is by spontaneous decay from the $^4F_{3/2}$ state. To calculate this, we begin by taking $\frac{N_2}{g_2}$ equal to twice the value found above, to account for the largest possible value of $\frac{N_4}{g_4}$. Since $g_2 = 2^{(6)}$, this gives us $N_2 = 2.1 \times 10^{18}/cm^3$. We approximate the value of N_2 for the 5 μseconds prior to the arrival of the laser pulse by this value. During this 5 μseconds, then, $(1 - e^{-\ell n\ 2 \times 5/360} = 0.01) \times 2.1 \times 10^{18}$ ions per cm^3 will have decayed to the N_4 level, i.e., the rate for one cm^3 is

approximately 4×10^{15} ions/μsecond. We now make the limiting assumption, that the rate of decay of the N_4 level is equal to lowest estimate of it, i.e., τ = 400 nanoseconds. With this assumption, we find that of the 4×10^{15} ions per cm^3 which decayed to the N_4 level in the first μsecond prior to the arrival of the pulse, only 2×10^{15} of them are still in the N_4 level when the pulse arrives. Of the 4×10^{15} ions per cm^3 which decayed to the N_4 level in the second μsecond, only 1×10^{14} of them are still in the N_4 level when the pulse arrives. At the very most, then, we see that the contribution to $\frac{N_4}{g_4}$ from decay of the $^4F_{3/2}$ level is 2×10^{15} ions/cm^3.

Adding this result, to the result from thermal equilibrium, we obtain: $\frac{N_4}{g_4} = 2 \times 10^{15} + 8 \times 10^{15} = 10^{16}/cm^3$. We observe that N_o, and hence $\frac{N_2}{g_2}$, is roughly 200 times this value.

APPENDIX III

DATA

(a) The first set of data presented here was obtained to determine the relationship between the electrical energy input to the flashlamp, and the amplifier pump energy, E (Figure 4-1). The energy E is determined as outlined in Section 3.3.1, from oscillograms of the flashlamp pulses. Each Polaroid frame has space for nine oscillograms or traces; this gives rise to the "trace numbers" listed below:

Frame No.	Trace No.	Elect. Energy Input (joules)	Pump Energy E (arbitrary units)	Remarks
a	2	67	90	For the oscillograms in this frame, only one of the four storage capacitors were connected to the flashlamp.
	4	100	131	
	5	133	156	
	6	166	175	
	7	200	211	
	8	83	110	
	9	117	145	
b	9	200	235	In this frame, as also in frame C and in traces 7 and 9 of frame d, 3 of the 4 storage capacitors were used.
	9	250	291	
	7	300	320	
	6	350	340	
	5	350	340	155 Oscilloscope sensitivity
	4	450	399	182 was changed here. These
	3	500	423	193 numbers are the energies
	2	550	440	201 E, before the corrections
	1	600	475	217 for this change were made.

Frame No.	Trace No.	Elect. Energy Input (joules)	Pump Energy E (arbitrary units)		Remarks
c	1	200	128 x f		The set-up of the apparatus was altered slightly between frames b and c. Consequently, this frame was used to find the multiplicative constant, f, relating the arbitrary units of frames a and b to those of c, d and e.
	3	300	149 x f		
	5	400	189 x f		
	7	500	208 x f		
	9	600	229 x f		
d	9	600	468	234	These numbers are the energies E before the multiplicative constant f is allowed for.
	7	700	486	243	
	5	400	402	201	In these traces, as in all the traces of frame e, all 4 of the storage capacitors were used.
	3	533	462	231	
	1	600	480	240	
e	9	666	494	247	
	7	733	540	270	
	5	800	562	281	
	3	867	582	291	
	1	933	588	294	

This completes the first set of data, giving the relation found in Figure (4-1).

(b) The next set of data was taken to provide energy gain measurements for the case in which the input pulse energy to the amplifier was 20 - 50 mullijoules. The pulse energies as recorded below, are corrected for the loss due to the beam splitter located in front of the thermopile. The amplifier pump energies E, recorded below, are obtained from the electrical energy input and the relation given in Figure (4-1).

Frame No.	Trace No.	Height of First Pulse (arbitrary units)	Pulse Energy Before Ampl. (milli-joules)	Pump Energy E (arbitrary units)	Pulse Energy AFter Ampl. (milli-joules)	Gain	Remarks
30	1	30.0	56.0	0	56.0	1.000	These oscillograms, to trace 6 of frame 37, were made to obtain the relation between the first pulse height, and the energy of the pulse before amplification. These data gives the relation shown in Figure (4-3).
	2	30.0	52.5				
	3	28.0	50.5				
	4	24.0	42.5				
	5	22.0	36.5				
	6	18.5	29.5				
	7	17.0	26.5				
33	5	18.0	25.5				
	6	25.5	46.0				
	7	25.0	42.0				
	8	23.0	38.5				
36	1	30.5	58.0				
37	2	31.0	54.5				
	3	30.0	53.0				
	4	24.0	40.0				
	5	23.0	38.5				
	6	16.0	22.5	0	22.5	1.000	
31	4	20.5	32.5	182	42.5	1.307	The "pulse energy before amplification" for these gain measurements (to trace 9 of frame 36) is obtained from Figure (4-3). These gain measurements form part of the data upon which Figure (4-4) is based.
	5	17.5	26.3	208	38.0	1.442	
32	1	18.0	27.0	92	35.5	1.315	
	2	22.5	37.0	110	46.0	1.242	
	3	16.0	24.0	125	30.0	1.251	
	4	16.0	24.0	142	32.0	1.335	
	5	14.0	21.5	155	28.0	1.301	
	6	23.0	38.5	170	48.0	1.246	
	7	13.0	20.5	195	27.5	1.341	
	8	22.0	35.0	92	38.0	1.057	
	9	23.0	38.5	110	48.0	1.247	
33	1	22.5	37.0	170	47.5	1.282	
	3	27.5	49.0	125	58.5	1.196	
	4	28.0	50.0	92	52.5	1.050	

Frame No.	Trace No.	Height of First Pulse (arbitrary units)	Pulse Energy Before Ampl. (milli-joules)	Pump Energy E (arbitrary units)	Pulse Energy After Ampl. (milli-joules)	Gain	Remarks
34	1	29.0	52.3	240	78.5	1.500	
	2	26.0	45.7	285	72.5	1.586	
	3	30.0	54.2	318	90.5	1.668	
	4	30.0	54.2	345	90.0	1.660	
	5	21.0	33.6	370	65.0	1.993	
	6	24.5	42.0	395	88.5	2.105	
	7	24.5	42.0	418	85.0	2.023	
	8	27.0	48.0	442	98.5	2.052	
	9	23.0	38.5	468	82.0	2.130	
35	1	27.0	48.0	480	101.0	2.105	
	2	23.5	40.0	455	85.0	2.125	
	3	21.0	33.6	430	69.0	2.052	
	4	24.0	41.0	407	82.0	2.000	
	6	25.0	43.3	358	78.0	1.802	
	7	21.0	33.6	330	59.0	1.753	
	8	24.0	41.0	300	70.0	1.708	
	9	23.0	38.5	262	63.0	1.638	
36	3	28.0	50.0	240	75.0	1.500	
	5	26.0	45.7	370	85.0	1.860	
	7	23.5	40.0	468	84.5	2.110	
	9	26.0	45.7	492	101.0	2.206	
38	8	31.5	58.0 x g	0	26.0	1.000	For these oscillograms, beginning with trace 8 of frame 38, the input pulse was attenuated from ∿ 40 mj. to ∿ 20 mj., in the hope that if saturation were occurring, it could be detected with this attenuation. Since it was not detected, it was decided that these results should be included with the previous
	9	31.5	58.0 x g	0	28.0	1.000	
41	5	31.0	57.0 x g	0	25.3	1.000	
39	1	27.3	22.8	468	42.3	1.860	
	2	26.2	21.7	442	39.3	1.810	
	3	26.2	21.7	418	40.0	1.845	
	4	29.0	24.6	395	41.4	1.680	
	5	27.3	22.8	370	38.0	1.668	
	6	30.0	25.6	345	41.4	1.620	
	7	27.8	23.4	318	36.0	1.540	
	8	27.3	22.8	285	33.4	1.465	
	9	28.0	23.5	240	31.0	1.320	

Frame No.	Trace No.	Height of First Pulse (arbitrary units)	Pulse Energy Before Ampl. (milli-joules)	Pump Energy E (arbitrary units)	Pulse Energy AFter Ampl. (milli-joules)	Gain	Remarks
40	1	23.0	18.1	262	28.0	1.547	ones, in a "20-50 mj.
	2	24.2	19.5	300	30.0	1.540	input pulse energy"
	3	30.0	25.6	330	40.0	1.562	class. Traces 8 and
	4	30.0	25.6	358	39.8	1.560	9 of frame 38, and
	5	26.7	22.2	382	37.6	1.695	trace 5 of frame 41,
	6	29.7	25.2	407	44.0	1.743	were used to find the
	7	23.2	18.4	430	34.3	1.862	attenuation factor, g.
	8	28.8	24.5	455	41.4	1.690	This factor g was then
	9	26.6	22.0	480	41.4	1.880	used to determine pulse energies before ampli-
41	6	16.7	11.8	170	13.3	1.126	fication for the
	7	17.0	12.0	125	12.6	1.050	remaining oscillograms
	8	23.2	18.6	110	18.9	1.020	to trace 9 of frame 41.
	9	24.0	19.3	92	22.0	1.140	
45	2	42.0	52.0	0	52.0	1.000	The attenuator was
	3	42.0	52.0				taken out at this
	4	41.0	48.0				point, and the
	5	36.5	43.0	0	43.0	1.000	arrangement of the
	6	23.0	26.0	0	26.0	1.000	unamplified pulse
	7	26.5	30.0				detector was changed
	8	18.0	21.0				slightly. This
	9	8.5	16.4				necessitated a new determination of the
46	1	8.5	16.0				relation between the
	2	19.0	22.3				first pulse height,
	3	27.5	32.5				and the energy of the
	5	30.0	32.7				pulse before ampli-
	6	34.0	40.0				fication. Thus, these
	7	39.0	46.4				oscillograms, from
	8	44.0	52.0				trace 2 of frame 45 to
	9	46.0	55.7	0	55.7	1.000	trace 8 of frame 64,
64	1	36.0	31.5				give the new relation, shown in Figure (4-5).
	2	36.0	32.0				
	3	49.3	45.0				
	5	39.2	36.0				
	6	38.0	35.0				
	7	29.0	25.0				
	8	20.8	19.0	0	19.0	1.000	

Frame No.	Trace No.	Height of First Pulse (arbitrary units)	Pulse Energy Before Ampl. (milli-joules)	Pump Energy E (arbitrary units)	Pulse Energy After Ampl. (milli-joules)	Gain	Remarks
65	3	46.4	56.0	240	79.0	1.412	The "pulse energies before amplification" for these gain measurements were obtained using the relation of Figure (4-5). These measurements, ending at trace 9 of frame 68, complete the set of data upon which Figure (4-4) is based.
	4	31.0	36.3	317	56.2	1.580	
	5	43.7	52.6	370	95.2	1.812	
	6	34.8	40.8	419	76.7	1.880	
	7	39.0	46.3	466	96.0	2.072	
	8	32.0	37.5	487	73.2	1.956	
	9	33.0	38.5	510	74.0	1.922	
66	1	22.0	26.6	532	51.3	1.930	
	2	32.6	38.1	522	78.0	1.050	
	3	36.7	44.0	500	93.2	2.120	
	4	21.0	25.6	477	50.7	1.975	
	5	32.0	37.5	455	71.2	1.900	
	6	33.4	39.0	442	72.7	1.860	
	7	36.3	43.0	395	80.0	1.860	
	8	39.0	46.3	345	84.7	1.830	
	9	36.0	42.5	285	69.2	1.630	
67	1	37.8	44.8	580	114.5	2.555	
	2	44.0	53.0	570	125.3	2.360	
68	1	42.0	50.3	467	116.0	2.300	
	2	36.2	42.7	498	101.2	2.370	
	3	40.0	47.5	522	108.0	2.280	
	4	43.2	52.0	542	118.5	2.280	
	5	39.5	47.0	562	108.0	2.300	
	6	38.0	45.0	560	104.0	2.310	
	7	37.5	44.5	580	109.3	2.450	
	8	39.0	46.3	589	108.0	2.335	
	9	42.3	50.7	592	130.6	2.585	

(c) The next set of data was taken to provide energy gain measurements, for the case in which the input pulse energy to the amplifier was 0.7-1.4 milli-joules. It was first necessary to relate the area of the second pulse in the oscillogram to the corresponding energy. The oscillograms on frames 45 and 46 are used to obtain the data for this; the resultant relation is shown in Figure (4-6).

Frame No.	Trace No.	Area of Second Pulse (arbitrary units)	Pulse Energy (milli-joules)	Frame No.	Trace No.	Area of Second Pulse (arbitrary units)	Pulse Energy (milli-joules)
45	2	260.0	52.0	46	1	88.0	16.0
	3	251.0	52.0		2	103.0	22.3
	4	249.5	48.0		3	155.5	32.5
	5	222.0	43.0		5	169.0	32.7
	6	126.0	26.0		6	217.5	40.0
	7	149.0	30.0		7	240.0	46.4
	8	98.0	21.0		8	295.0	52.0
	9	82.5	16.4		9	286.0	55.7

The thin C_uSO_4 attenuator was then put in place, and the sensitivity of the oscilloscope was increased by a factor of 10. The slope of the relation in Figure (4-6), divided by 10, gives the "pulse energy after amplification" in the data given below. In the data given below, the oscillograms from trace 4 of frame 52 to trace 2 of frame 55 were used to find the attenuation factor h. In the remaining data, from trace 5 of frame 52 to trace 1 of frame 55, the "pulse energy before amplification" was found by using this attenuation coefficient. These remaining data constitute the gain measurements upon which Figure (4-7) is based.

Frame No.	Trace No.	Height of First Pulse (arbitrary units)	Pulse Energy Before Ampl. (milli-joules)	Pump Energy E (arbitrary units)	Area of Second Pulse (arbitrary units)	Pulse Energy After Ampl. (milli-joules)	Gain
52	4	39.5	47.5 x h	0	101.0	2.00	1.000
53	1	42.0	50.5 x h	0	100.0	2.00	
	2	38.0	45.5 x h	0	80.8	1.61	
	3	37.3	44.5 x h	0	90.0	1.80	
	4	29.5	33.5 x h	0	62.0	1.23	

Frame No.	Trace No.	Height of First Pulse (arbitrary units)	Pulse Energy Before Ampl. (milli-joules)	Pump Energy E (arbitrary units)	Area of Second Pulse (arbitrary units)	Pulse Energy After Ampl. (milli-joules)	Gain
55	1	42.0	50.5 x h	0	53.0	1.05	1.000
52	5	26.8	1.156	100	68.5	1.36	1.178
	7	15.0	0.720	157	50.8	1.00	1.390
53	9	15.0	0.720	92	41.0	0.81	1.125
54	1	19.2	0.842	92	55.0	1.09	1.294
	2	18.3	0.815	125	56.0	1.11	1.360
	3	24.0	1.040	240	76.0	1.50	1.440
	6	24.6	1.060	420	112.5	2.24	2.110
	7	15.2	0.728	467	65.0	1.29	1.775
	8	25.6	1.106	280	83.0	1.65	1.490
	9	32.0	1.408	345	118.0	2.35	1.665
55	3	20.3	0.878	455	82.0	1.63	1.860
	4	31.3	1.367	332	111.0	2.20	1.606
	5	26.3	1.127	263	81.0	1.61	1.428
	6	14.0	0.701	442	63.0	1.25	1.780
	7	22.1	0.958	395	79.0	1.57	1.640
	8	18.0	0.797	370	74.5	1.48	1.860
	9	25.0	1.080	319	86.0	1.70	1.577

(d) The next and final set of data was taken to provide energy gain measurements, for the case in which the input pulse energy to the amplifier was 0.05 - 0.12 millijoules. It was necessary to increase the sensitivity of the amplified pulse detector by removing some of the protective cardboard shielding surrounding it. This was done, the sensitivity of the oscilloscope was decreased, and the following oscillograms were taken in order to determine the new relation between the area of the second pulse and the amplified pulse energy:

Frame No.	Trace No.	Height of First Pulse (arbitrary units)	Pulse Energy Before Ampl. (milli-joules)	Pump Energy E (arbitrary units)	Area of Second Pulse (arbitrary units)	Pulse Energy After Ampl. (milli-joules)	Gain
57	1	31.7	1.533	0	162.0	1.533	1.000
	2	27.9	1.307		150.0		
	3	24.0	1.130		114.3		
	5	40.8	2.060		128.0		
	6	19.0	0.910		49.3		
	7	14.2	0.770		42.2		
	8	23.7	1.118		58.8		
	9	10.0	0.700	0	39.8	0.700	1.000

It is this date which yields the relation shown in Figure (4-8).

The thin C_uSO_4 filter was then replaced by the thick one, and the oscilloscope sensitivity was increased by a factor of ten. In the data given below, the oscillograms from trace 2 of frame 58 to trace 8 of frame 63 were used to determine the new attenuation factor, j. This factor was used to find the "pulse energy before amplification" in the remaining oscillograms, to obtain the data upon which Figure (4-9) is based.

Frame No.	Trace No.	Height of First Pulse (arbitrary units)	Pulse Energy Before Ampl. (milli-joules)	Pump Energy E (arbitrary units)	Area of Second Pulse (arbitrary units)	Pulse Energy AFter Ampl. (milli-joules)	Gain
58	2	16.6	20.0 x j	0	76.2	0.070	1.000
	3	19.0	22.0 x j		84.2	0.077	
	4	26.7	30.0 x j		97.7	0.089	
	5	32.0	37.2 x j		106.8	0.098	
62	8	15.1	19.2 x j		67.5	0.062	
	9	38.2	45.8 x j		137.3	0.126	

Frame No.	Trace No.	Height of First Pulse (arbitrary units)	Pulse Energy Before Ampl. (milli-joules)	Pump Energy E (arbitrary units)	Area of Second Pulse (arbitrary units)	Pulse Energy After Ampl. (milli-joules)	Gain
63	3	33.6	19.2 x j		114.2	0.105	
	4	16.0	19.7 x j	0	73.5	0.067	1.000
	5	16.0	19.7 x j		70.2	0.064	
	6	26.2	30.0 x j		78.8	0.072	
	7	19.5	22.5 x j		72.2	0.065	
	8	13.0	18.0 x j	0	66.3	0.061	1.000
58	7	22.2	.0771	318	142.3	0.131	1.698
	8	10.0	.0519	370	107.9	0.099	1.909
	9	16.6	.0613	419	129.0	0.118	1.921
59	1	27.5	.0960	301	157.0	0.144	1.500
	2	15.2	.0590	262	103.8	0.095	1.610
	3	11.1	.0537	442	119.3	0.1095	2.045
	5	18.4	.0660	345	120.8	0.1173	1.775
	6	19.6	.0691	285	109.0	0.100	1.445
	8	23.6	.0830	370	159.7	0.146	1.760
	9	15.4	.0598	240	95.3	0.0985	1.460
60	1	26.2	.0918	331	168.6	0.145	1.580
	3	17.2	.0630	383	126.0	0.1156	1.835
	4	20.6	.0724	407	142.2	0.130	1.796
	5	16.7	.0613	430	120.0	0.110	1.793
	6	15.8	.0599	442	127.2	0.1167	1.954
	7	13.2	.0559	455	117.7	0.108	1.940
62	1	26.7	.0928	92	117.2	0.107	1.156
	2	32.0	.1145	100	138.3	0.126	1.106
	3	31.2	.1107	109	132.0	0.121	1.093
	4	18.2	.0645	117	81.0	0.074	1.147
	5	17.2	.0630	125	82.0	0.075	1.190

APPENDIX IV

COMPUTER PROGRAMS

The program which follows is typical of the programs used to obtain the least squares fits, given in Figures (4-4), (4-7), (4-9), and (5-1). The method used to minimize the residual sum of squares,

$$\Sigma(y - e^{A(1 - e^{-\gamma x})})^2$$

where $y = G_E$,

$A = 0.30 \times \sigma \times L \times N_{go}$

and $x = E$

is to reduce its derivative with respect to γ to zero by successive iterations. In the case in which σ was set equal to $10^2 \times \sigma_{given}$ in Figure (5-1), limitations of the computer necessitated replacing $(1 - e^{-\gamma x})$ by γx.

```
03504  MASHALIDIS I.   040                    FØRTRAN SØURCE LIST
       ISN        SØURCE STATEMENT

     0 $IBFTC
     1         DIMENSIØN X(90),Y(90),EXPR(9),SUM1(9),SUM2(9),RSSQ(9),GA(9)
     2       3 FØRMAT (1X,//)
     3       4 FØRMAT (1X,10H BAD Y IS ,E13.6,5X,9HBAD X IS ,E13.6)
     4       5 FØRMAT (1X,9H SUM1 IS ,E13.6,5X,8HEXPR IS ,E13.6)
     5       8 FØRMAT (1X,23HSTD WITH FINAL GAMMA IS,E13.6)
     6       6 FØRMAT (10X,5HGAMMA,10X,4HRSSQ)
     7       7 FØRMAT (1X,7H GAMMA=,E13.6,5X,6H RSSQ=,E13.6)
    10      10 FØRMAT (I3)
    11       9 FØRMAT (2X,7HFØR E =,E13.6,9HGAIN IS  ,E13.6)
    12      11 FØRMAT (F6.3,F6.1)
    13      54 FØRMAT (1X,10HFØR GAMMA=,E13.6,5HRSSQ=,E13.6)
    14      53 FØRMAT (1X,2HY=,F6.3,2HX=,F6.1,7HCALC Y=,F6.3)
    15         JUG=1
    16      55 JUG=JUG+1
    17         READ (5,10) N
    21         DØ 30 I=1,N,1
    22         READ (5,11) Y(I),X(I)
    23         IF (2.8-Y(I)) 15,15,30
    24      14 IF (X(I)-1.0) 15,15,30
    25      15 WRITE (6,4) Y(I),X(I)
    26         WRITE (6,3)
    27      30 CØNTINUE
    31         M=1
    32         A=26.5
    33         G=0.00006
    34         GUMP=0.00005
    35      12 SUM1(M)=0.
    36         SUM2(M)=0.
    37         RSSQ(M)=0.
    40         TRSQ=0.0
    41         DØ 20 I=1,N
    42         SUM1(M)=SUM1(M)+X(I)*EXP(A-G*X(I)-2.0*A*EXP(-G*X(I)))
    43         SUM2(M)=SUM2(M)+X(I)*Y(I)*EXP(-G*X(I)-A*EXP(-G*X(I)))
    44         RSSQ(M)=RSSQ(M)+(Y(I)-EXP(A-A*EXP(-G*X(I))))**2
    45         TRSQ=TRSQ+(Y(I)-EXP(A-A*EXP(-GUMP*X(I))))**2
    46         IF (M-7) 18,19,18
    47      19 GNA=EXP(A-A*EXP(-G*X(I)))
    50         WRITE (6,53) Y(I),X(I),GNA
    51      18 CØNTINUE
    52      20 CØNTINUE
    54         EXPR(M)=SUM1(M)-SUM2(M)
    55         IF (EXPR(M)) 51,52,51
    56      52 EXPR(M)=EXPR(M)+0.100000E-14
    57      51 CØNTINUE
    60         WRITE (6,3)
    61         WRITE (6,54) GUMP,TRSQ
    62         WRITE (6,3)
    63         GUMP=GUMP+0.0000012
    64         GA(M)=G
    65         G=G*((SUM1(M)-EXPR(M))/SUM1(M))**2
    66         M=M+1
    67         IF (M-8) 12,12,21
    70      21 AB=N
    71         STD=SQRT(RSSQ(8)/(AB-1.0))
```

```
03504  MASHALIDIS I.   040                          FØRTRAN SØURCE LIST
       ISN          SØURCE STATEMENT

         72           DØ 22 I=50,800,50
         73           D=I
         74           RES=EXP(A-A*EXP(-G*D))
         75           WRITE (6,9) D,RES
         76        22 CØNTINUE
        100           WRITE (6,3)
        101           DØ 31 I=1,8,1
        102           WRITE (6,5) SUM1(I),EXPR(I)
        103           WRITE (6,7) GA(I),RSSQ(I)
        104           WRITE (6,3)
        105        31 CØNTINUE
        107           WRITE (6,8) STD
        110           WRITE (6,3)
        111           IF (JUG-5) 55,55,40
        112        40 CØNTINUE
        113           STØP
        114           END
```

```
FØR GAMMA= 0.500000E-04RSSQ= 0.310808E 01

FØR GAMMA= 0.512000E-04RSSQ= 0.259426E 01

FØR GAMMA= 0.524000E-04RSSQ= 0.215611E 01

FØR GAMMA= 0.536000E-04RSSQ= 0.179708E 01

FØR GAMMA= 0.548000E-04RSSQ= 0.152073E 01

FØR GAMMA= 0.560000E-04RSSQ= 0.133075E 01

Y= 1.307X= 182.0CALC Y= 1.320
Y= 1.422X= 208.0CALC Y= 1.373
Y= 1.315X=  92.0CALC Y= 1.151
Y= 1.242X= 110.0CALC Y= 1.183
Y= 1.251X= 125.0CALC Y= 1.210
Y= 1.335X= 142.0CALC Y= 1.242
Y= 1.301X= 155.0CALC Y= 1.267
Y= 1.246X= 170.0CALC Y= 1.296
Y= 1.341X= 195.0CALC Y= 1.346
Y= 1.057X=  92.0CALC Y= 1.151
```

Y= 1.247X= 110.0CALC Y= 1.183
Y= 1.282X= 170.0CALC Y= 1.296
Y= 1.196X= 125.0CALC Y= 1.210
Y= 1.050X= 92.0CALC Y= 1.151
Y= 1.500X= 240.0CALC Y= 1.441
Y= 1.586X= 285.0CALC Y= 1.543
Y= 1.668X= 318.0CALC Y= 1.621
Y= 1.660X= 345.0CALC Y= 1.689
Y= 1.933X= 370.0CALC Y= 1.753
Y= 2.105X= 395.0CALC Y= 1.820
Y= 2.023X= 418.0CALC Y= 1.884
Y= 2.052X= 442.0CALC Y= 1.953
Y= 2.130X= 468.0CALC Y= 2.030
Y= 2.105X= 480.0CALC Y= 2.067
Y= 2.125X= 455.0CALC Y= 1.991
Y= 2.052X= 430.0CALC Y= 1.918
Y= 2.000X= 407.0CALC Y= 1.853
Y= 1.802X= 358.0CALC Y= 1.722
Y= 1.753X= 330.0CALC Y= 1.651
Y= 1.708X= 300.0CALC Y= 1.578
Y= 1.638X= 262.0CALC Y= 1.490
Y= 1.500X= 240.0CALC Y= 1.441
Y= 1.860X= 370.0CALC Y= 1.753
Y= 2.110X= 468.0CALC Y= 2.030
Y= 2.206X= 492.0CALC Y= 2.104
Y= 1.860X= 468.0CALC Y= 2.030
Y= 1.810X= 442.0CALC Y= 1.953
Y= 1.845X= 418.0CALC Y= 1.884
Y= 1.680X= 395.0CALC Y= 1.820
Y= 1.668X= 370.0CALC Y= 1.753
Y= 1.620X= 345.0CALC Y= 1.689
Y= 1.540X= 318.0CALC Y= 1.621
Y= 1.465X= 285.0CALC Y= 1.543
Y= 1.320X= 240.0CALC Y= 1.441
Y= 1.547X= 262.0CALC Y= 1.490
Y= 1.540X= 300.0CALC Y= 1.578
Y= 1.562X= 330.0CALC Y= 1.651
Y= 1.560X= 358.0CALC Y= 1.722
Y= 1.695X= 382.0CALC Y= 1.785
Y= 1.743X= 407.0CALC Y= 1.853
Y= 1.862X= 430.0CALC Y= 1.918
Y= 1.690X= 455.0CALC Y= 1.991
Y= 1.880X= 480.0CALC Y= 2.067
Y= 1.342X= 170.0CALC Y= 1.296
Y= 1.252X= 125.0CALC Y= 1.210
Y= 1.320X= 92.0CALC Y= 1.151
Y= 1.126X= 170.0CALC Y= 1.296
Y= 1.050X= 125.0CALC Y= 1.210
Y= 1.140X= 92.0CALC Y= 1.151
Y= 1.412X= 240.0CALC Y= 1.441
Y= 1.580X= 317.0CALC Y= 1.619
Y= 1.812X= 370.0CALC Y= 1.753
Y= 1.880X= 419.0CALC Y= 1.887
Y= 2.072X= 466.0CALC Y= 2.024
Y= 1.956X= 487.0CALC Y= 2.089
Y= 1.922X= 510.0CALC Y= 2.161
Y= 1.930X= 532.0CALC Y= 2.233
Y= 2.050X= 522.0CALC Y= 2.200

```
Y= 2.120X= 500.0CALC Y= 2.129
Y= 1.975X= 477.0CALC Y= 2.058
Y= 1.900X= 455.0CALC Y= 1.991
Y= 1.860X= 442.0CALC Y= 1.953
Y= 1.860X= 395.0CALC Y= 1.820
Y= 1.830X= 345.0CALC Y= 1.689
Y= 1.630X= 285.0CALC Y= 1.543
Y= 2.555X= 580.0CALC Y= 2.398
Y= 2.360X= 570.0CALC Y= 2.363
Y= 2.300X= 467.0CALC Y= 2.027
Y= 2.370X= 498.0CALC Y= 2.123
Y= 2.280X= 522.0CALC Y= 2.200
Y= 2.280X= 542.0CALC Y= 2.267
Y= 2.300X= 562.0CALC Y= 2.335
Y= 2.310X= 570.0CALC Y= 2.363
Y= 2.450X= 580.0CALC Y= 2.398
Y= 2.335X= 589.0CALC Y= 2.431
Y= 2.585X= 592.0CALC Y= 2.441


FØR GAMMA= 0.572000E-04RSSQ= 0.123095E 01



FØR GAMMA= 0.584000E-04RSSQ= 0.122527E 01


 FØR E = 0.500000E 02GAIN IS   0.107958E 01
 FØR E = 0.100000E 03GAIN IS   0.116523E 01
 FØR E = 0.150000E 03GAIN IS   0.125741E 01
 FØR E = 0.200000E 03GAIN IS   0.135657E 01
 FØR E = 0.250000E 03GAIN IS   0.146324E 01
 FØR E = 0.300000E 03GAIN IS   0.157794E 01
 FØR E = 0.350000E 03GAIN IS   0.170127E 01
 FØR E = 0.400000E 03GAIN IS   0.183384E 01
 FØR E = 0.450000E 03GAIN IS   0.197631E 01
 FØR E = 0.500000E 03GAIN IS   0.212939E 01
 FØR E = 0.550000E 03GAIN IS   0.229383E 01
 FØR E = 0.600000E 03GAIN IS   0.247043E 01
 FØR E = 0.650000E 03GAIN IS   0.266007E 01
 FØR E = 0.700000E 03GAIN IS   0.286365E 01
 FØR E = 0.750000E 03GAIN IS   0.308215E 01
 FØR E = 0.800000E 03GAIN IS   0.331662E 01


 SUM1 IS  0.353331E-06     EXPR IS  0.864239E-08
 GAMMA= 0.600000E-04      RSSQ= 0.137118E 01


 SUM1 IS  0.330739E-06     EXPR IS -0.298090E-08
 GAMMA= 0.571007E-04      RSSQ= 0.123569E 01
```

```
SUM1 IS  0.338619E-06      EXPR IS  0.102888E-08
GAMMA= 0.581346E-04       RSSQ= 0.121822E 01

SUM1 IS  0.335909E-06      EXPR IS -0.355637E-09
GAMMA= 0.577819E-04       RSSQ= 0.121620E 01

SUM1 IS  0.336847E-06      EXPR IS  0.122888E-09
GAMMA= 0.579043E-04       RSSQ= 0.121595E 01

SUM1 IS  0.336523E-06      EXPR IS -0.424762E-10
GAMMA= 0.578621E-04       RSSQ= 0.121592E 01

SUM1 IS  0.336635E-06      EXPR IS  0.146834E-10
GAMMA= 0.578767E-04       RSSQ= 0.121592E 01

SUM1 IS  0.336596E-06      EXPR IS -0.509104E-11
GAMMA= 0.578716E-04       RSSQ= 0.121592E 01

STD WITH FINAL GAMMA IS 0.119603E 00
```

REFERENCES

1. Ambartsumyan, R.V., Basov, N. G., Zuev, V.S., Kryuknov, P.G., and Letokov, V.S., "Propagation of a Light Pulse in a Non-Linearly Amplifying and Absorbing Medium", Soviet Phys. JETP Letters, 4, p. 12 - 16, 1966.
2. Borelli, N.F., and Charters, M.L., "Energy Distribution in a Glass: Nd^{3+} Laser Rod", J. Appl. Phys., 36, 2172 - 4, 1965.
3. Cabezas, A.Y., McAllister, G.L., and Ng, W.K., "Gain Saturation in Neodymium: Glass Laser Amplifiers", J. Appl. Phys., 38, p. 3487 - 91, 1967.
4. Chaio, R.Y., Garmire, E., and Townes, C.H., "Self-Trapping of Optical Beams", Phys. Rev. Letters, 13, p. 479 - 82, 1964.
5. Diecke, G.H., "Spectroscopic Observations on Maser Materials", in Advance in Quantum Electronics, edited by J.R. Singer, Columbia University Press, New York, 1961.
6. Hill, K.O., Giant Pulse Evolution in a Nd^{3+}-Glass Q-Switched Laser, Ph.D. Thesis, McMaster University, 1968.
7. Korobkin, V.V., and Serov, R.V., "Investigation of Self-Focusing of Neodymium-Laser Radiation", Soviet Phys. JETP Letters, 6, p. 135 - 7, 1967.
8. Lengyel, B.A., Introduction to Laser Physics, (John Wiley and Sons, Inc., New York, 1966).
9. Michon, M., "The Influence of Nd^{3+} Ion Properties in a Glass Matrix on the Dynamics of a Q-Spoiled Laser", I.E.E.E. J. of Quantum Electronics, QE-2, p. 612 - 616, 1966.

10. Michon, M., Ernest, J., Hanus, J., and Auffret, R., "Influence of the $4I^{11/2}$ Level Lifetime on the Effective Use of the Population Inversion in a Q-Spoiled Neodymium Doped Glass Laser", Phys. Letters, 19, p. 219 - 20, 1965.

11. Michon, M., Ernest, J., Dumanchin, R., Hanus, J., and Raynard, S., "On the Spectral Properties of a Q-Switched Nd^{3+} Doped Laser Emission", Phys. Letters, 19, p. 217 - 19, 1965.

12. Schuldt, S. B., and Aagard, R.L., "An Analysis of Radiation Transfer by Means of Elliptical Cylinder Reflectors", Appl. Optics, 2, p. 509 - 513, 1963.

13. Steele, E.L., Optical Lasers In Electronics, (John Wiley and Sons, Inc., New York, 1968).

14. Steele, E.L., and Davis, W.C., "Laser Amplifiers", J. of Appl. Phys., 36, p. 348 - 352, 1965.

15. Littel, K.F., and Chernock, J.P., "Gain-Delay Characteristics of a Pulsed Neodymium-Glass Laser Oscillator-Amplifier Chain", Proc. of the I.E.E.E., 53, p. 82 - 83, 1965.